A divergent *Plasmodium* NEK4 acts as a key regulator driving the early events of meiosis

Ryuji Yanase[1, 2], Molly Hair[3], Mohammad Zeeshan[1], David J. P. Ferguson[3], Declan Brady[1], Carla Pasquarello[4], Andrew Bottrill[5], Suhani Bhanvadia[6], Arrmund Neal[6], Eelco C. Tromer[7], Karine G. Le Roch[6], Alexandre Hainard[4], Anthony A. Holder[8], Sue Vaughan[3], David S. Guttery[1, 2, *], Rita Tewari[1, *]

[1]School of Life Sciences, Queen's Medical Centre, University of Nottingham, Nottingham, UK
[2]Department of Genetics, Genomics and Cancer Sciences, College of Life Sciences, University of Leicester, Leicester, UK
[3]Oxford Brookes University, Department of Biological and Medical Sciences, Oxford, UK
[4]Proteomics Core Facility, Faculty of Medicine, University of Geneva, Switzerland
[5]School of Life Sciences, Gibbet Hill Campus, University of Warwick, Coventry, UK
[6]Department of Molecular, Cell and Systems Biology, University of California, Riverside, Riverside, United States
[7]Cell Biochemistry, Groningen Institute of Biomolecular Sciences & Biotechnology, University of Groningen, Groningen, The Netherlands
[8]Malaria Parasitology Laboratory, The Francis Crick Institute, London, UK

*Corresponding authors:
rita.tewari@nottingham.ac.uk (RT); david.guttery@nottingham.ac.uk (DSG)

Abstract

Meiosis is a conserved yet evolutionarily varied process underpinning sexual reproduction in eukaryotes. In the malaria parasite *Plasmodium*, meiosis is unconventional: it occurs immediately after fertilisation (post-zygotic) and must be coordinated with the transformation of the zygote into a motile ookinete. The mechanisms synchronising these meiotic and morphogenetic programmes remain unknow. Here, we identify the *Plasmodium berghei* NIMA-related kinase, NEK4 as a key regulator that couples meiotic initiation with zygote morphogenesis. Using ultrastructure expansion microscopy, we show that NEK4 accumulates at the microtubule-organising centre (MTOC) and the apical polar complex (APC) shortly after fertilisation, preceding the assembly of perinuclear and cortical microtubules. We reveal that *Plasmodium* zygotes undergo a nuclear migration driven by the MTOC, analogous to the horsetail nuclear movement of fission yeast. Deletion of *nek4* results in complete developmental arrest: MTOC duplication and microtubule formation are blocked, chromatin remains uncondensed, and nuclear migration and cell polarity fail to establish. Transcriptomic and phosphoproteomic analyses reveal that NEK4 absence causes a collapse in transcriptional and phosphoregulatory networks governing meiosis and cytoskeletal organisation, leading to reduced expression and phosphorylation of important players, including HOP1, REC8, and AP2-O. These findings establish NEK4 as a key regulator driving meiotic entry and zygote maturation.

Keywords: *Plasmodium*; meiosis; NIMA-related kinase; malaria; zygote; ookinete; MTOC; microtubules; chromosome

Introduction

Meiosis is a conserved and essential mode of cell division that underpins sexual reproduction in eukaryotes. It entails a carefully choreographed sequence of events, including DNA replication, homologous recombination, synapsis and two rounds of chromosome segregation[1]. In mammals, it generates haploid gametes from diploid progenitors, following two successive nuclear divisions without intervening genome duplication[1]. In many well-studied organisms including yeast, plants, and mammals, meiotic progression is regulated by a network of conserved protein kinases and checkpoints, including cyclin-dependent kinases (CDKs), Polo-like kinases (PLKs), the anaphase-promoting complex/cyclosome (APC/C), ataxia-telangiectasia mutated (ATM)/ATM and Rad3-related (ATR) kinases, checkpoint kinases (CHK1/2), and members of the NIMA-related kinase (NEK) family[2, 3, 4, 5]. These regulators ensure the fidelity of chromosome segregation by integrating signals from DNA damage checkpoints, spindle dynamics, and crossover/recombination status, at the same time as maintaining synchrony with cytoskeletal changes that support cell division and differentiation.

Despite the broad conservation of its core function to facilitate obligatory chromosomal exchanges and homologous recombination between parental chromosomes, both the molecular machinery executing meiosis and its operational sequence of events display remarkable variability[6, 7]. For a wide range of unicellular eukaryotes, including parasitic protists, meiotic programmes have undergone substantial evolutionary divergence. This is evident in the malaria-causing parasite *Plasmodium*, a member of the phylum Apicomplexa[7, 8]. This haploid parasite has a complex lifecycle with proliferative asexual multiplication in the liver and blood stream of the host[9]. A subpopulation of blood-stage parasites differentiates into haploid male and female gametocytes which, following ingestion in a mosquito blood meal, start the sexual phase of the life cycle inside the gut of the vector. Gametogenesis produces haploid gametes and following fertilisation, meiosis occurs in the diploid zygote; a process known as post-zygotic meiosis. The zygote undergoes a ~24-hour developmental programme to become an elongated, motile ookinete capable of traversing the midgut epithelium[8] (Fig. 1a), where it forms an oocyst. Many haploid sporozoites then emerge from the oocyst, migrate to the mosquito salivary glands and transmit to the vertebrate host in the blood meal. *Plasmodium* infections result in over 250 million clinical cases and nearly 600,000 deaths each year, disproportionately affecting young children in sub-Saharan Africa[10]. These outcomes are driven not only by the rapid asexual proliferation in the human host, but also by the successful

78 sexual reproduction and transmission through the mosquito vector. Transmission is an obligate
79 part of the life cycle and therefore prevalence of the disease is critically reliant on the process
80 of meiosis[9].
81
82 Early meiotic events, for example DNA replication, chromosome pairing, and formation of
83 chromosome axes, are initiated within the first few hours post-fertilisation. Ultrastructural
84 studies have shown that *Plasmodium* zygotes progress through early prophase I stages, forming
85 distinct synaptonemal complexes (SC) that persists unusually until anaphase I. However, later
86 prophase stages and meiosis II are not observed[11, 12]. Despite two rounds of chromosome
87 segregation, the ookinete retains a single nucleus with four kinetochore clusters, indicating a
88 divergent closed meiosis without karyokinesis[13].
89
90 The cell biological divergence of meiosis is reflected at the molecular level as well.
91 *Plasmodium* species lacks orthologues of several conserved meiotic regulators, including
92 CDC25, CDC14, PLKs, and many APC/C components[14, 15]. They do possess a reduced,
93 parasite-specific set of protein kinases that appear to have acquired regulatory roles normally
94 fulfilled by these missing elements[15, 16]. The signalling mechanisms that control *Plasmodium*
95 meiosis and coordinate with cytoskeletal reorganisation and establishment of cell polarity, are
96 poorly defined, although cGMP signalling has been suggested to initiate ookinete gliding
97 motility and polarization[17]. One protein kinase family of particular interest is the NIMA-
98 related kinases (NEKs), which are conserved across eukaryotes and regulate centrosome
99 function, spindle assembly, and 3D chromatin organisaion[18, 19]. In metazoans, specific NEKs
100 such as NEK1, NEK2, and NEK9 function in meiosis and mitosis, often through regulation of
101 microtubule dynamics and DNA damage (NEK1) and spindle assembly (NEK2 and NEK9)
102 checkpoint control[18, 20]. The *Plasmodium* genome encodes four NEKs (NEK1–4), which have,
103 apart from *Plasmodium* NEK1 and human NEK2, no direct 1-to-1 human orthologs (Extended
104 Data Fig. 1a, b). Each *Plasmodium* NEK has a distinct expression pattern and function during
105 the parasite life cycle[21, 22, 23, 24], with NEK2 and NEK4 shown to be critical for zygote
106 development and parasite transmission[15, 21] (Extended Data Fig. 1c). Deletion of *nek4* gene
107 results in a failure of DNA replication in the zygote following fertilisation and a complete block
108 in ookinete formation at the early stage of meiosis[21] (Figure 1a), yet the underlying function
109 and phosphosignalling network remain undefined.
110

111 Here, we show that during early zygote development where the post-zygotic meiosis
112 commences, *Plasmodium berghei* (Pb) NEK4 is located at the microtubule organising centre
113 (MTOC) and apical polar complex (APC). Deletion of the *nek4* gene disrupts microtubule
114 organisation, MTOC development, and nuclear migration during meiotic S phase and prophase.
115 Furthermore, its absence impairs transcription and phosphorylation of key meiotic proteins,
116 leading to a failure in chromosome condensation and developmental arrest at the earliest stages
117 of meiosis. We propose that this kinase integrates the nuclear and cell differentiation events
118 that drive meiotic progression and ookinete development, respectively.
119

120 Results

121 NEK4 moves to the nucleus, MTOC, and apical polar complex during early meiotic 122 development

123 Our previous study showed that NEK4 ablation blocks zygote development[21]. To investigate
124 NEK4 functions during the meiotic stages of *P. berghei* development, first we determined the
125 spatiotemporal location of NEK4, using a transgenic parasite line expressing the protein with
126 a C-terminal GFP tag from the modified endogenous gene locus (PbNEK4-GFP – Extended
127 Data Fig. 1d-f). Live-cell imaging revealed a dynamic pattern of PbNEK4-GFP location
128 following female gametocyte activation, zygote differentiation and ookinete development (Fig.
129 1b and Extended Data Fig. 2). In non-activated female gametocytes, the GFP signal was
130 diffused throughout the nucleoplasm and cytoplasm (Fig. 1b). Then in the first two hours post-
131 activation (hpa) and shortly after fertilisation, the PbNEK4-GFP signal was concentrated in
132 two foci (Fig. 1b), one at the periphery of the nucleus near the nuclear envelope and the other
133 at the cell cortex. By two to six hpa, these foci were more pronounced, suggesting a dual
134 location of PbNEK4-GFP at both nuclear and apical regions of the cell during this period of
135 intense morphological transformation. The PbNEK4-GFP signal within the nucleoplasm
136 appeared stronger relative to the cytoplasm. In addition, a focal dot-like PbNEK4-GFP-positive
137 structure was observed moving around in the cytoplasm (Fig. 1b; yellow arrowhead), and this
138 was often still visible even after the cell had fully transformed into an ookinete. The
139 morphological transformation of the zygote into an ookinete begins at about 4 hpa and is
140 initiated at the site where PbNEK4-GFP is located at the cell periphery. The onset of this
141 transformation is accompanied by reduction of this GFP signal and the disappearance of the
142 nuclear PbNEK4-GFP focus, with residual PbNEK4-GFP dispersed diffusely throughout the
143 cytoplasm and nucleoplasm (Fig. 1b, c).

144

145 To examine in more detail the location of NEK4 within the developing zygote, we used
146 ultrastructure expansion microscopy (U-ExM). NHS-ester staining of cells at 2 hpa revealed
147 the nuclear MTOC and the development of the APC at the cell periphery. Immunofluorescence
148 labelling of the U-ExM samples with an anti-GFP antibody confirmed that PbNEK4-GFP was
149 located at both the MTOC and the APC (Fig. 1d). Furthermore, at 4 hpa, the dividing and
150 separating MTOCs and a more developed APC were observed by NHS-ester staining. At this
151 later time point, a distinct presence of PbNEK4-GFP at both the MTOCs and the APC was
152 confirmed (Fig. 1d). These observations indicate that the prominent location of NEK4 during
153 the early stages of zygote development (2 to 4 hpa), with a concentration at the MTOC and
154 APC, alongside a diffuse distribution within the nucleoplasm (Fig. 1e).

155

156 **NEK4 drives nuclear repositioning and directional microtubule formation in the zygote**

157 In our study of NEK4 localisation in early meiotic zygotes, we observed that the nucleus shows
158 dynamic movement during early meiosis as seen across various eukaryotes[6, 25, 26]. For example,
159 in the fission yeast *Schizosaccharomyces pombe* (*S. pombe*), nuclear movement during meiosis
160 is characterised by a dramatic "horsetail" motion, where the nucleus oscillates back and forth
161 along the cell axis during prophase I[27, 28]. This movement is driven by cytoplasmic dynein and
162 microtubules anchored at the spindle pole body (SPB)[29, 30], and is essential for efficient
163 homologous chromosome pairing and recombination[27]. Time-lapse imaging of PbNEK4-GFP
164 zygotes at 2 hpa revealed that inside the zygote, PbNEK4-GFP focus localised at the nucleus
165 and moves together with the nucleus (magenta arrowheads in Fig. 2a and Supplementary Video
166 1, 2). To examine MTOC and microtubule dynamics in parallel during the nuclear movement,
167 we used a transgenic PbEB1-GFP parasite line[31], in which PbEB1-GFP marks the microtubule
168 lattice and the MTOC[31, 32]. The PbEB1-GFP focus, representing the MTOC position, was
169 observed moving within the zygote, leading the nucleus (magenta arrowheads in Fig. 2b). The
170 nucleus appeared elongated, seemingly pulled by the PbEB1-GFP focus. Additionally, PbEB1-
171 GFP signal was observed extending from the focus, likely representing microtubules extending
172 from the MTOC (Fig. 2b and Supplementary Video 3, 4). Furthermore, the fact that the
173 localisation of PbNEK4-GFP and PbEB1-GFP at the cell periphery remains largely stationary
174 contrasts with the nuclear movement (cyan arrowheads in Fig. 2a and b), indicating that this
175 nuclear movement is independent of whole-cell rotation or migration.

176

177 Quantification of the proportion of zygotes at different stages during development with motile
178 nuclei indicated that the movement peaked at between 2 and 4 hpa and then subsided (Fig. 2c).
179 These observations suggest that in *P. berghei* zygotes there is a form of nuclear movement like
180 that widely observed in *S. pombe* and other eukaryotes[6, 25, 26, 27, 33]. This movement appears to
181 be led by the MTOC, where both PbNEK4-GFP and PbEB1-GFP are located (Fig. 2d).
182
183 To investigate the microtubule structures at higher resolution during the early development
184 stages, we performed U-ExM using an anti-α-tubulin antibody (Fig. 2e and Extended Data Fig.
185 3a-c). At 2 hpa, two populations of zygotes were present: those with a single MTOC and those
186 with duplicated MTOCs. In cells with a single MTOC (Fig. 2e, top left panel), multiple
187 microtubules were visible in the perinuclear region, with one microtubule oriented as if
188 extending from the nuclear MTOC toward the APC. In cells with duplicated MTOCs (Fig. 2e,
189 top right panel), both microtubules emanating from the MTOCs and microtubule organisation
190 at the APC appeared more developed. Some of the microtubules running along the nuclear
191 periphery appeared to connect to the APC. In zygotes at 4 hpa (Fig. 2e, bottom left panel), the
192 two MTOCs were separating, with a microtubule structure resembling a spindle oriented
193 between them. Further development of microtubule structures was also evident in the
194 perinuclear region and at the APC. In summary, significant microtubule development occurs
195 at both the nuclear MTOCs and the APC, the sites of greatest PbNEK4-GFP accumulation (Fig.
196 2f), suggesting that NEK4 may be involved in regulating microtubule polymerisation or
197 dynamics. This association of NEK4 with the MTOC and APC suggests a function as a spatial
198 organiser of microtubule polarity in the developing zygote. The microtubules extending around
199 the nucleus appear analogous to the perinuclear microtubules observed in other eukaryotes
200 during early meiosis, which mediate nuclear and chromosome movement[27, 34].
201
202 **NEK4 is essential for nuclear migration, microtubule formation, and morphological**
203 **transformation from zygote to ookinete**
204 To assess the importance of NEK4 during zygote/meiotic development, we used an existing
205 *nek4* gene knockout parasite line (*Pbnek4-ko*; Extended Data Fig. 4a, b)[21]. A previous study
206 has shown that while *Pbnek4-ko* parasites undergo fertilisation, subsequent DNA replication
207 and ookinete formation are blocked[21]. Live-cell imaging over the period between 2 to 24 hpa
208 confirms that *Pbnek4-ko* zygotes failed to elongate or transition through the retort form into
209 mature ookinetes, in contrast to PbNEK4-GFP control cells that completed this transformation
210 within 20 hours (Fig. 3a). We then investigated the nuclear movement observed in zygotes.

211 Although moving nuclei were observed in a few *Pbnek4-ko* zygotes between 2 and 4 hpa, the
212 proportion of cells with moving nuclei was significantly reduced compared to the PbNEK4-
213 GFP controls (Fig. 3b).
214
215 To investigate microtubules in *Pbnek4-ko* zygotes, we used U-ExM. This revealed that the
216 distinctive formation of perinuclear and APC-associated microtubules in WT cells was almost
217 completely ablated in *Pbnek4-ko* zygotes (Fig. 3c). Although the presence of some tubulin was
218 detected, the formation of the microtubule-based structures at the APC was almost completely
219 disrupted compared to PbNEK4-GFP controls (WT; Fig. 3c). Additionally, while the formation
220 of a nuclear MTOC was observed, it failed to duplicate and remained as a single MTOC over
221 the first four hours after fertilisation. Together, these data on the consequences of *nek4* gene
222 deletion demonstrate that NEK4 is essential for MTOC duplication and the organisation of
223 perinuclear and apical microtubule networks. These processes are prerequisites for DNA
224 replication, meiotic entry, and morphological transition from zygote to ookinete. In the absence
225 of NEK4, the microtubule-based cytoskeletal framework necessary for meiotic progression
226 fails to assemble, leading to developmental arrest prior to transition to retort form (Fig. 3d).
227
228 **NEK4 is essential for establishing the ultrastructure necessary for meiotic chromatin**
229 **condensation and APC development**
230 To examine the ultrastructural consequences of *Pbnek4* knockout, we used transmission
231 electron microscopy (TEM) to study WT and *Pbnek4-ko* zygotes at 2 hpa and 4 hpa (Fig. 4a).
232 In WT zygotes at 2 hpa, the APC structure was observed at the cell periphery, along with its
233 associated microtubules (Fig. 4a1-2), and perinuclear microtubules were detected around the
234 nucleus (Fig. 4a3-4). While *Pbnek4-ko* zygotes had also initiated APC formation with
235 microtubules at the cell periphery at 2 hpa, the APC was smaller and only partially formed
236 (Fig. 4a5-6). Perinuclear microtubules were detected in only few *Pbnek4-ko* zygotes (Fig. 4a7-
237 8).
238
239 At 4 hpa, WT zygotes had a developed APC with a well-organised microtubule structure (Fig.
240 4a9-10). At this stage, multiple thread-like structures were observed within the nucleus
241 (magenta arrowheads, Fig. 4a11-13). These are likely condensed leptotene chromosomes,
242 marking the entry into meiosis, and the ends of these chromosomes appeared to be attached to
243 the nuclear envelope (Fig. 4a13). In contrast, *Pbnek4-ko* zygotes at 4 hpa had only small APC

244 and microtubule structures (Fig. 4a14-15) and the condensed chromosomes seen in WT zygotes
245 were completely absent in *Pbnek4-ko* zygotes (Fig. 4a16-18).
246
247 To examine further the ultrastructural differences between WT and *Pbnek4-ko* zygotes, we
248 used Serial Block-Face Scanning Electron Microscopy (SBF-SEM). In most WT zygotes at 4
249 hpa, a developed APC was detected (Fig. 4b, c) and multiple condensed, thread-like
250 chromosomes were detected within their nuclei (Fig. 4b, magenta arrowheads and inset). In
251 some zygotes, these chromosomes were observed pairing with linear structures between them,
252 indicative of likely synaptonemal complex formation (Fig. 4b, cyan arrowheads and inset). In
253 contrast, in *Pbnek4-ko* zygotes at 4 hpa there was impaired APC development, and no
254 condensed chromosomes nor synaptonemal complexes were present within the nucleus (Fig.
255 4b, c). Three-dimensional models constructed from the SBF-SEM datasets illustrate the
256 development of the APC, the formation of condensed chromosomes (with one or both ends
257 appearing to attach to the nuclear envelope), and the separation of MTOCs in WT zygotes at 4
258 hpa. All these early meiotic processes are blocked in *Pbnek4-ko* zygotes (Fig. 4d). These
259 findings indicate that the deletion of the *Pbnek4* gene not only severely impairs the
260 development of the APC and its associated microtubule network in the early zygote but also
261 ablates the formation of condensed chromosomes (likely leptotene chromosomes), which is a
262 critical step for meiotic entry.
263
264 **NEK4 drives meiotic entry by coordinated control of transcription, protein synthesis and**
265 **phosphorylation**
266 To elucidate the molecular processes governed by NEK4 during early meiosis in *P. berghei*
267 zygote development, we performed an integrated transcriptomic, proteomic,
268 phosphoproteomic, and interactomic analysis. Global transcriptomics was conducted on WT
269 and *Pbnek4-ko* parasites at 2 hpa. and quantitative proteomics/phosphoproteomics were
270 conducted on non-activated and 2 hpa samples for both WT and *Pbnek4-ko* parasites. GFP-
271 Trap interactomics was performed using PbNEK4-GFP parasites at 2 hpa.
272
273 Quantitative real-time PCR (qRT-PCR) showed that the expression of meiosis-related genes
274 (e.g., *dmc1*, *hop1*, *mnd1*, and *spo11*) was significantly downregulated in *Pbnek4-ko* zygotes at
275 2 hpa compared to WT zygotes at 2 hpa (Extended Data Fig. 5a). Transcriptomic profiling via
276 RNA-sequencing between WT and *Pbnek4-ko* parasites at 2 hpa revealed major transcriptional
277 changes in *Pbnek4-ko* parasites. At 2 hpa, 1,554 genes were significantly differentially

278 expressed (adjusted p-value ≤ 0.05, fold change ≥ 2) relative to WT parasites, comprising 717
279 downregulated and 837 upregulated genes (Fig. 5a; Supplementary Table 1). Gene Ontology
280 enrichment of downregulated transcripts highlighted key biological processes, including cell
281 motility, cell differentiation, meiotic nuclear division, and cytoskeletal organisation –
282 hallmarks of zygote maturation (Fig. 5b; Supplementary Table 2). Notably, transcripts
283 encoding the meiotic recombinase *dmc1* and the putative synaptonemal complex component
284 *hop1* (PBANKA_1407900) were strongly reduced in the *Pbnek4-ko* line.
285
286 Next, we performed GFP pulldown assays using PbNEK4-GFP and WT-GFP zygotes at 2 hpa.
287 This analysis identified interactions of PbNEK4-GFP with putative MTOC-associate proteins,
288 such as a PI3K/PI4K catalytic domain-containing protein (PBANKA_0806700) and a MORN
289 repeat protein (PBANKA_1030400), as well as a regulator of chromosome condensation
290 (RCC; PBANKA_0905500). Furthermore, interactions with meiotic factors, including REC8
291 (PBANKA_1419300), DMC1, and HOP1, were also indicated (Fig. 5c; Supplementary Table
292 13). These interactions may suggest that NEK4 acts as a signalling hub, and either directly
293 phosphorylates or stabilises other components within an integrated meiotic complex.
294
295 To investigate the full landscape of NEK4-associated protein abundance and phosphorylation
296 changes during early zygote development, we performed quantitative proteomics and
297 phosphoproteomics analyses using non-activated (0 hpa) WT and *Pbnek4-ko* gametocytes, and
298 WT and *Pbnek4-ko* zygotes at 2 hpa. Initial analysis of phosphopeptide-enriched and flow-
299 through fractions from *Pbnek4-ko* and WT gametocytes at 0 hpa revealed minimal differences
300 in the abundance of identified proteins and phosphopeptides (Extended Data Fig. 5b and d;
301 Supplementary Table 5 and 12). This suggests that *Pbnek4* deletion has little impact on the
302 protein or phosphorylation status of gametocytes prior to activation.
303
304 In contrast, significant differences in protein and phosphopeptide abundance were observed
305 when comparing gametocytes at 0 hpa with zygotes at 2 hpa, and *Pbnek4-ko* with WT zygotes
306 at 2 hpa (Fig. 5d-g; Extended Data Fig. 5c and f; Supplementary Table 6 and 11). Proteomic
307 analysis of the flow-through fractions obtained during phosphopeptide enrichment revealed
308 marked increases in zygote- and meiosis-associated proteins following fertilisation in WT
309 parasites. These included the zinc-finger protein Pb103[35], the transcription factor AP2-Z[36], and
310 the meiotic recombinase DMC1[37] (Fig. 5d; Supplementary Table 3). In contrast, when *Pbnek4-*
311 *ko* parasites were compared to WT controls at 2 hpa, many of these same proteins were

312 significantly less abundant (Fig. 5e; Supplementary Table 4), suggesting that NEK4 activity is
313 required for their synthesis, stability, or translation during zygote development.
314
315 Phosphoproteomic profiling revealed a similar association with the presence of NEK4 for
316 protein phosphorylation linked to meiotic initiation. In WT parasites, fertilisation triggered
317 widespread phosphorylation of proteins linked to meiosis, transcription, translation, and
318 cytoskeletal organisation by 2 hpa. These proteins included DMC1[37], HOP1, REC8, DNA
319 polymerase delta subunit 3 (POLD3), AP2-Z[36, 38], AP2-O[39], Pb103[35], FD2[40], gSNF2[41], NOT1-
320 G[42], PI3K/PI4K, serine/threonine protein kinase putatively related to MAP/microtubule
321 affinity-regulating kinase 1[43] and maternal embryonic leucine zipper kinase 1[44]
322 (MARK/MELK), zygote-ookinete specific dynein heavy chain (DHC3)[45], and kinesin-4
323 (KIN4) (Fig. 5f; Supplementary Table 5). In *Pbnek4-ko* parasites phosphorylation at many sites
324 in these proteins was significantly lower relative to the WT control (Fig. 5g; Supplementary
325 Table 9), Notably, some of these proteins also showed increased overall abundance in the flow-
326 through fraction (e.g. DMC1, Pb103, and AP2-Z), indicating that the observed phosphorylation
327 changes may partly reflect higher protein levels rather than phosphorylation alone. However,
328 the consistent reduction of phosphorylation in *Pbnek4-ko* parasites suggests that NEK4
329 contribute to phosphoregulation in addition to promoting protein accumulation. Gene Ontology
330 (GO) analysis further confirmed that zygote activation triggers increased phosphorylation of
331 proteins involved in microtubule-based movement, the cytoskeleton, and reproductive
332 processes (Fig. 5h; Supplementary Table 8). In contrast, *Pbnek4-ko* zygotes at 2 hpa showed
333 reduced phosphorylation of proteins associated with reproductive processes and meiotic
334 nuclear division (Fig. 5i; Supplementary Table 10). Representative proteins identified by our
335 proteomics and phosphoproteomic analyses, along with their abundance and putative functions,
336 are summarised in Figure 5j. These data support the hypothesis that NEK4 may contributes to
337 a phosphorylation network underpinning zygote differentiation and meiotic progression.
338
339 Collectively, these integrated transcriptomic, interactomic, proteomic, and phosphoproteomic
340 datasets suggest that NEK4 provides control at multiple regulatory levels. Together with the
341 evidence from the transcriptomic and interactomic studies, these results identify NEK4 as a
342 key regulator of early post-zygotic meiosis in *P. berghei*, orchestrating the integrated control
343 of transcription, protein abundance and phosphosignalling to drive meiotic entry and zygote
344 maturation.
345

346 ## Discussion

347 We identify NEK4 as a pivotal kinase coordinating meiotic initiation and zygote
348 morphogenesis in *P. berghei* (Fig. 6). NEK4 is located at both the MTOC and the APC during
349 the earliest stages of zygote development (post-zygotic meiosis), and orchestrates MTOC
350 duplication, perinuclear and APC microtubule formation, and migration of the nucleus. This
351 directed movement resembles the "horsetail" nuclear oscillations during the meiotic prophase
352 in other eukaryotes, where cytoskeleton-driven repositioning of the nucleus promotes
353 homologous chromosome pairing and recombination[27, 33]. In *S. pombe*, this nuclear movement
354 occurs during prophase, where linear elements (LinEs) mediate chromosome pairing and
355 crossover. Similarly, in *Plasmodium*, from ~4 hpa onwards —when DNA replication is
356 complete, nuclear movement is evident, and morphological transformation into the ookinete
357 begins —the formation of condensed chromosomes reminiscent of leptotene chromosomes and
358 structures resembling synaptonemal complexes were observed. This suggests that entry into
359 meiotic prophase initiates at this stage in *Plasmodium* (Fig. 6). In the absence of NEK4, the
360 MTOC fails to duplicate, chromatin remains diffuse, and nuclear translocation is lost, leading
361 to arrest of cell development before meiotic division and transformation to ookinete. These
362 data suggest that NEK4 is a putative central regulator linking nuclear reorganisation and
363 cytoskeletal polarity at the onset of meiosis. Previous studies suggest that while *Plasmodium*
364 retains some canonical meiotic processes well-characterised in organisms like *S. pombe*, its
365 mechanisms and molecular players are highly divergent, as evidenced by the evolutionary
366 conservation analysis of meiotic components in *Plasmodium* and by the progression through
367 meiosis I and II without nuclear division[8] (Fig. 6). Given this divergence, it is particularly
368 intriguing that early meiotic nuclear movement observed in model eukaryotes is conserved in
369 *Plasmodium*, suggesting that it may be important for homologous chromosome pairing and
370 recombination in this parasite as well.
371
372 The dual location of NEK4 and the developmental arrest that results from knocking out its
373 gene, place it at the intersection of nuclear and cytoskeletal organisation. Its behaviour parallels
374 that of NEKs in other systems, which regulate centrosome duplication, spindle formation, and
375 checkpoint transitions[18, 19]. In *S. pombe*, the NEK-like kinase Fin1 controls spindle formation,
376 specifically the maturation and inheritance of the SPB[46, 47], while NEK2 and NEK9 act at
377 metazoan centrosomes to coordinate spindle assembly[19]. In *Plasmodium*, which lacks
378 canonical mitotic and meiotic regulators such as the phosphatases CDC25, CDC14, and Polo-

379 like kinases[14, 15], NEK4 appears to have acquired functions to integrate both signalling and
380 structural control within a simplified regulatory network.
381
382 Proteins identified in the PbNEK4-GFP pulldown assays, such as the PI3K/PI4K catalytic
383 domain-containing protein (PBANKA_0806700), MORN repeat protein
384 (PBANKA_1030400), and Kinesin-4 (PBANKA_1208200), may interact with NEK4 at the
385 MTOC to facilitate MTOC development or segregation. Additionally, the identified regulator
386 of chromosome condensation (RCC; PBANKA_0905500) contains an RCC1 domain and
387 likely functions through interaction with chromosomes or DNA. Interestingly, human NEK8
388 and NEK9 possess an RCC1 domain, and the RCC1 domain is implicated in the recruitment to
389 the centrosome[48]. This raises the possibility that the *Plasmodium* RCC identified here is
390 similarly recruited to the MTOC, where it may interact with NEK4 to execute MTOC-
391 associated functions.
392
393 Transcriptomic, proteomic and phosphoproteomic profiling revealed that fertilisation triggers
394 extensive reprogramming of transcript, protein abundance, and protein phosphorylation during
395 post-zygotic meiosis. In WT parasites, proteins likely essential for meiosis and zygote
396 differentiation including protein sets relating to meiosis (DMC1, HOP1 and REC8), DNA
397 replication (POLD3), sexual development (Pb103, AP2-Z, NOT1-G, FD2, AP2-O, gSNF2),
398 and MTOC/microtubules (PIK/PIK4, MARK/MELK, DHC3, KIN4) are more phosphorylated
399 in the zygote (Fig. 6). In *Pbnek4-ko* parasites, these proteins were hypophosphorylated,
400 suggesting that NEK4 plays a role in phosphorylation events required for onset of meiosis and
401 zygote-ookinete development. Also, the reduction both in protein abundance and
402 phosphorylation for some proteins (e.g. DMC1, Pb103, and AP2-Z) suggests a dual-level of
403 control in which NEK4 promotes both synthesis and activation of key meiotic regulators.
404
405 Such coordinated phosphoregulation is consistent with broader concepts being developed for
406 eukaryotic meiosis. Recent phosphoproteomic studies in yeast have shown that meiotic
407 progression is driven by both changes in protein abundance and dynamic, stage-specific waves
408 of protein phosphorylation that rewire existing signalling networks[49]. These phosphorylation
409 cascades, directed by cyclin-dependent and Polo-like kinases, define temporal transitions from
410 recombination to segregation[49]. Large-scale quantitative phosphoproteomics studies in *S.*
411 *pombe* revealed that phosphorylation of thousands of sites changes during meiotic
412 development, for example affecting proteins involved in microtubule organisation,

413 recombination and chromosome cohesion[50]. Our findings are consistent with this concept of a
414 meiotic "phosphorewiring": the absence of NEK4 collapses a broad phosphorylation
415 programme encompassing transcriptional, translational and cytoskeletal effectors, and
416 implying that *Plasmodium* has an analogous, temporally-ordered kinase programme despite its
417 highly reduced kinase signalling repertoire.
418
419 Our structural observations suggest that the APC and the microtubules extending from the
420 nuclear MTOC are formed in a NEK4-dependent manner. Furthermore, we observed a link
421 between the microtubules extending from the MTOC and APC, suggesting that this connection
422 is associated with nuclear movement or positioning. Comparable architectures are present in
423 other apicomplexans: in *Toxoplasma gondii*, the APC and conoid form an anchoring hub that
424 coordinates cortical microtubules and organelle positioning[51, 52]. *Eimeria tenella* and
425 *Cryptosporidium* spp. also have similar apical scaffolds[53, 54]. Genetic modification has resulted
426 in comparable defects in other apicomplexans, supporting a conserved requirement for precise
427 coordination between nuclear and cortical assembly. In *T. gondii*, conditional mutants of NEK1
428 and the MAP kinase, MAPK2 block centrosome duplication and segregation, causing the
429 nucleus to replicate without successful daughter cell budding, effectively decoupling nuclear
430 and cytoskeletal programmes[55, 56]. *Plasmodium* NEK1 controls spindle and kinetochore
431 organisation during male gametogenesis[24], while loss of the phosphatase PPKL disrupts apical
432 complex integrity and ookinete morphogenesis[14, 57]. A putative MARK/MELK-related
433 serine/threonine protein kinase (PBANKA_1305200), identified in our phosphoproteomics
434 analysis, may be directly or indirectly activated by NEK4 to stimulate microtubule-associated
435 proteins, thereby promoting or stabilising microtubule formation at the APC and MTOC in the
436 zygote. Together, these studies highlight a recurrent feature of Apicomplexa: kinases and
437 phosphatases govern centrosome and apical organisation, and their perturbation uncouples
438 nuclear and cortical events, resulting in developmental arrest. The function of NEK4 fits within
439 this broader mechanistic framework, acting as a linchpin to preserve synchrony between
440 meiotic and morphogenetic processes.
441
442 The perinuclear microtubules observed in early zygotes may be involved in the nuclear
443 movement described above and intranuclear chromosome movement (Fig. 6). In *S. pombe*,
444 horsetail nuclear movement is driven by SPB-derived microtubules interacting with the cell
445 cortex via dynein[29, 30]. We speculate that a similar mechanism generates nuclear movement in
446 *Plasmodium*, through the interaction of perinuclear microtubules with dynein (e.g, DHC3,

447 which was identified in our phosphoproteomics). Furthermore, in eukaryotes including mice,
448 nematodes, and yeast, it is well established that meiotic chromosomes interact with dynein on
449 perinuclear microtubules via the SUN/KASH complex on the nuclear envelop, facilitating
450 chromosome movement and pairing[58]. Given that SUN proteins localise to the nuclear envelope
451 during the zygote-to-ookinete development in *Plasmodium*[59], it is plausible that SUN proteins
452 mediate the interaction between chromosomes and dynein on perinuclear microtubules, thereby
453 driving intranuclear chromosome movement to promote homologous chromosome pairing.
454
455 In an evolutionary context, NEK4 exemplifies how *Plasmodium* has condensed but not
456 abandoned a central feature of meiotic control, to ensure synchrony between nuclear and
457 cytoskeletal events. The parasite has a compact kinome, and a limited number of four NEKs
458 have diversified to perform additional discrete yet complementary roles: for example, NEK1
459 regulates spindle formation during male gametogenesis[24], while NEK4 governs meiotic
460 initiation and zygote differentiation. This division of labour underscores the adaptive flexibility
461 of NEKs in the absence of canonical Polo-kinases and other regulators. The NEK4 regulatory
462 module may be a *Plasmodium*-specific version of an ancient, conserved solution to a universal
463 cellular problem – to use specific waves of phosphorylation to coordinate chromosomal
464 replication with structural reorganisation of the cell during meiosis.
465
466 In conclusion, NEK4 functions as a key regulator that co-ordinates meiotic entry in
467 *Plasmodium*, coupling microtubule organisation, MTOC duplication, nuclear migration, DNA
468 replication, and chromosome condensation with the establishment of apical polarity (Fig. 6).
469 By integrating translational and phosphoregulatory control, NEK4 ensures that nuclear and
470 cytoskeletal events are synchronised to drive zygote morphogenesis and meiosis. These
471 findings clarify the molecular requirements of meiosis in Apicomplexa, highlighting a
472 conserved principle – kinase-mediated coordination of nuclear and cellular processes – that
473 extends across the eukaryotic kingdom. Given that NEK4 is essential for the development of
474 transmission-stage parasites and the absence of close orthologs from the human host, this
475 kinase represents a promising transmission-blocking therapeutic target. NEK4 provides a
476 window to investigate how the minimalist signalling networks of divergent parasites sustain
477 their complex developmental programmes.
478

479 # Methods

480 **Ethics statement**

481 All animal experiments were conducted in the United Kingdom in accordance with the Animals
482 (Scientific Procedures) Act 1986 and approved by the Home Office under Project Licence
483 numbers PDD2D5182 and PP3589958. Protocols were reviewed and approved by the
484 institutional Animal Welfare and Ethical Review Body (AWERB) prior to implementation.
485 Procedures were designed to minimise animal suffering and the number of animals used, in
486 line with the 3Rs (Replacement, Reduction, Refinement) principles. Experiments were
487 performed on female CD1 outbred mice aged 6 to 8 weeks, housed under standard conditions
488 with environmental enrichment and monitored daily for health and welfare.

489

490 **Generation of transgenic parasites**

491 For C-terminal GFP-tagging of NEK4 (PBANKA_0616700) by single crossover homologous
492 recombination, a 930 bp region of *nek4* downstream of the ATG start codon was amplified
493 using primers 5'-CCCCGGTACCGATAGCGATAAGAGAGTAAGATTGTGTG-3' and 5'-
494 CCCCGGGCCCAACATCAACAATATCCAATAATAATG-3' (Supplementary Table 8).
495 Genotype analysis was performed using integration PCR as illustrated in Extended Data Fig.
496 1d. Primer 1 (intNEK4: 5'-CCAACCATATATTACACAGAGGTTAG-3') and primer 2
497 (ol492)[14] were used to confirm correct integration of the *gfp* sequence at the target locus. *P.*
498 *berghei* ANKA line 2.34 parasites were then transfected by electroporation[60]; confirmation of
499 the correct protein size was performed by Western blot analysis[24]. Production of the *Pbnek4-*
500 *ko* parasite line has been described previously[15, 21].

501

502 **Live cell imaging**

503 To analyse PbNEK4-GFP expression during the zygote to ookinete transition, gametocytes or
504 zygotes activated in ookinete culture medium were purified by Nycodenz gradient[15]. Hoechst
505 33342 was added to stain nuclear DNA. Zygote and ookinete development were tracked for up
506 to 24 hours post-fertilisation to assess the dynamics of PbNEK4-GFP location during meiotic
507 progression and morphogenesis. Images were captured on a Zeiss Axio Imager M2 microscope
508 equipped with a 63× oil immersion objective and an AxioCam ICc1 digital camera (Carl Zeiss).
509 Fluorescence signals from GFP and Hoechst were prone to bleaching, but imaging conditions
510 were optimised to ensure sufficient resolution to follow protein dynamics across key
511 developmental transitions. Axiovision software (Rel. 4.8) was used to enhance contrast and

512 minimise background, ensuring threshold settings remained consistent across samples.
513 Representative images from at least three independent biological replicates are presented, with
514 protein location assessed in 30–50 individual cells per time point.
515
516 **Transmission electron microscopy**
517 For ultrastructural analysis of NEK4-deficient and wild-type parasites, zygotes were harvested
518 at 2 and 4 hpa and fixed in 4% glutaraldehyde in 0.1 M phosphate buffer. Samples were
519 processed for transmission electron microscopy following the protocol described in the
520 previous study[61]. Briefly, fixed cells were post-fixed in osmium tetroxide, stained en bloc with
521 uranyl acetate, dehydrated through a graded ethanol series, and embedded in Spurr's epoxy
522 resin. Ultrathin sections (approximately 70 nm) were cut using a diamond knife, mounted on
523 copper grids, and stained with uranyl acetate followed by lead citrate to enhance contrast.
524 Sections were examined using a Tecnai G2 12 BioTwin (FEI UK, UK) or a JEOL 1200EX
525 transmission electron microscope (JEOL, Japan) operated at 100 kV. Representative images
526 were captured digitally for analysis.
527
528 **Serial block face scanning electron microscopy (SBF-SEM) of zygotes at 4 hpa**
529 Samples were processed for SBF-SEM following the protocol described previously[62].
530 Fractions enriched in WT and *Pbnek4-ko* zygotes at 4 hpa were fixed at room temperature in
531 4% glutaraldehyde in 0.1 M phosphate buffer. Samples were then spun and washed three times
532 in 0.1 M phosphate buffer, and post-fixed in 1% osmium tetroxide in 1.5% potassium
533 ferrocyanide in 0.1 M phosphate buffer (for 45 min at room temperature, and in the dark). After
534 the first osmium step, samples were washed three times in 0.1 M phosphate buffer, incubated
535 in 1% tannic acid in 0.1 M phosphate buffer for 30 min at room temperature, and then subjected
536 to a second osmium step (2% OsO_4 in ddH_2O, for 30 min, at room temperature, and in the
537 dark). Samples were then incubated in 2% uranyl acetate in ddH_2O for 2 h, dehydrated in
538 acetone (a progressive series of acetone concentrations from 20%, 40%, 90% to 100% with
539 three changes in molecular-sieved ultradry acetone over 4 h) and embedded in TAAB 812 Hard
540 resin (TAAB, catalogue number T030). The tips of resin blocks containing samples were
541 trimmed and mounted onto aluminium pins using conductive epoxy glue and silver dag, and
542 then sputter coated with a layer (10–13 nm) of gold, in an Agar Auto Sputter Coater (Agar
543 Scientific). Before SBF-SEM imaging, ultrathin sections (70 nm) of the block face were
544 examined in a Jeol JEM 1400 Flash transmission electron microscope (JEOL), to verify sample
545 quality. Samples were then imaged in a Merlin VP compact high resolution scanning electron

546 microscope (Zeiss) equipped with a 3View stage (Gatan-Ametek), and an OnPoint back-
547 scattered electron detector (Gatan-Ametek), in variable pressure. The following imaging
548 conditions were used: 2 kV, 20 µm aperture, 30 pascal variable pressure, 2 nm pixel size, 5 µs
549 pixel time, 100 nm section thickness, 100% FCC.
550
551 **Ultrastructure expansion microscopy**
552 Ultrastructure expansion microscopy (U-ExM) was performed on PbNEK4-GFP non-activated
553 gametocytes or zygotes at 2 or 4 hpa, following previously published protocols with slight
554 modifications[63, 64]. Parasites were fixed in 4% formaldehyde in MTSB buffer (10 mM MES,
555 150 mM NaCl, 5 mM EGTA, 5 mM $MgCl_2$, 5 mM glucose, pH7.0) and adhered to 10 mm
556 poly-D-lysine–coated round coverslips for 15 min. Coverslips were incubated overnight at 4°C
557 in 1.4% formaldehyde (FA)/2% acrylamide (AA). Gelation was performed in ammonium
558 persulphate/TEMED (10% each)/monomer solution (23% sodium acrylate; 10% AA; 0.1%
559 BIS-AA in PBS) on ice for 5 min and at 37°C for 30 min. Gels were denatured for 15 min at
560 37°C and for 90 min at 95°C in denaturation buffer (200 mM SDS, 200 mM NaCl, 50 mM
561 Tris, pH 9.0, in water). After denaturation, gels were incubated in distilled water overnight for
562 complete expansion. The next day, circular gel pieces with a diameter of ∼13 mm were excised,
563 and the gels were washed in PBS three times for 15 min to remove excess water. The gels were
564 then incubated in blocking buffer (3% BSA in PBS) at room temperature for 30 min, incubated
565 with rabbit polyclonal anti-GFP antibody (1:250 dilution; A11122; Invitrogen) or mouse
566 monoclonal anti-α-tubulin antibody (1:500 dilution: T9026; Sigma-Aldrich) in blocking buffer
567 at 4°C overnight, and washed three times for 15 min in wash buffer (0.5% vol/vol Tween-20
568 in PBS). The gels were incubated with 8 µg/ml Atto 594 NHS-ester (Merck), 10 µg/ml Hoechst
569 33342 (Molecular Probes), and Alexa Fluor 488 goat anti-rabbit IgG (A11008; Invitrogen) or
570 Alexa Fluor 488 goat anti-mouse IgG (A11001; Invitrogen) in PBS (1:500 dilution) at 37°C
571 for 2.5 h followed by three washes of 15 min each in wash buffer (blocking and all antibody
572 incubation steps were performed with gentle shaking). The gels were then washed three times
573 for 15 min with wash buffer and expanded overnight in ultrapure water. The expanded gel was
574 placed in a 35-mm glass-bottom dish (MatTek) with the 14-mm glass coated with poly-D-
575 lysine. High-resolution images were acquired on a Zeiss Celldiscoverer 7 with Airyscan using
576 a 50×/1.2 water objective. Confocal z-stacks were acquired using line scanning and the
577 following settings: 55 × 55 nm pixel size, 170-nm z-step, 2.91 µs/pixel dwell time, 850 gain,
578 and 3.5% (405 nm), 4.5% (488 nm), and 5.0% (561 nm) laser powers. The z-stack images were
579 processed and analysed using Fiji (version 1.54f). Each experiment was repeated at least three

580 times, and protein localisation was assessed in 10 cells per condition. Full imaging details are
581 provided in the figure legends.
582
583 **Quantitative real-time PCR (qRT-PCR) analysis**
584 Total RNA was extracted from WT and *Pbnek4-ko* zygotes at 2 hpa (three biological replicates
585 per condition) using the RNA Purification Kit (Stratagene), and cDNA was synthesised using
586 the RNA-to-cDNA Kit (Applied Biosystems). qPCR was performed with 80 ng of RNA using
587 SYBR Green Fast Master Mix (Applied Biosystems) on an Applied Biosystems 7500 Fast
588 system. Cycling conditions were: 95 °C for 20 s, followed by 40 cycles of 95 °C for 3 s and
589 60 °C for 30 s. Primers were designed using Primer3 (https://primer3.ut.ee/). Each gene was
590 tested in three biological and technical replicates. *hsp70* (PBANKA_081890) and *arginyl-*
591 *tRNA synthetase* (PBANKA_143420) were used as reference genes. Primer sequences are
592 listed in Supplementary Table 14.
593
594 **Transcriptome study using RNA-Sequencing**
595 RNA samples from WT and *Pbnek4-ko* zygotes at 2 hpa (three biological replicates per
596 condition) were vacuum-concentrated by freeze drying and transported in RNA-stabilising
597 tubes (Biomatrica) to ensure preservation. Strand-specific mRNA libraries were prepared using
598 the TruSeq Stranded mRNA Library Prep Kit LT (Illumina). Paired-end sequencing (2 × 150
599 bp) was performed on an Illumina HiSeq 4000 platform. Quality control of raw sequencing
600 reads was carried out using FASTQC
601 (http://www.bioinformatics.babraham.ac.uk/projects/fastqc). Adapter trimming and removal
602 of low-quality sequences were performed using Trimmomatic. Cleaned reads were aligned to
603 the *P. berghei* ANKA reference genome (PlasmoDB release 40) using HISAT2 version 2.1.0,
604 applying the parameter --rna-strandness FR. Gene-level expression was quantified using
605 FeatureCounts. Raw read counts were converted to counts per million (CPM), and genes with
606 CPM <1 in all but one replicate were excluded from downstream analysis. Library sizes were
607 normalised using the trimmed mean of M-values (TMM) method in the EdgeR package.
608 Processed count data were then analysed using the voom transformation from the limma
609 package to model the mean–variance relationship. Differential expression analysis was
610 performed with DESeq2, using a false discovery rate (FDR)-adjusted p-value threshold of 0.05
611 (Benjamini–Hochberg correction) and a fold-change cut-off of ≥2 to define significantly
612 regulated genes.
613

614 **Immunoprecipitation and mass spectrometry**

615 Purified gametocytes from WT-GFP and PbNEK4-GFP parasites were activated for 2 h and
616 proteins were crosslinked using 1% formaldehyde for 10 min at room temperature. Excess
617 aldehyde was quenched by incubating samples in 0.125 M glycine for 5 min, followed by three
618 washes with PBS (pH 7.5). Immunoprecipitation of PbNEK4-GFP complexes was performed
619 using the GFP-Trap_A kit (Chromotek) in accordance with the manufacturer's protocol. GFP-
620 bound protein complexes were captured on beads and processed for liquid chromatography–
621 tandem mass spectrometry (LC-MS/MS). Beads were washed and incubated in ammonium
622 bicarbonate (ABC) buffer. Reduction and alkylation were carried out using 10 mM TCEP
623 (tris(2-carboxyethyl)phosphine hydrochloride) and 40 mM chloroacetamide (CAA) for 5 min
624 at 70°C. Proteins were then digested with trypsin overnight at room temperature (1 µg trypsin
625 per 100 µg of protein). Digestion was halted by adjusting the pH to 3–4 with 1% trifluoroacetic
626 acid (TFA) before mass spectrometry analysis. Tryptic peptides were analysed via LC-MS/MS.
627 Resulting raw data were searched using FragPipe version 21.0 (https://fragpipe.nesvilab.org/)
628 against the PlasmoDB-66_PbergheiANKA_AnnotatedProteins database. Search parameters
629 included trypsin digestion with up to two missed cleavages, fixed carbamidomethylation of
630 cysteines, and variable modifications for methionine oxidation and N-terminal acetylation.
631 Protein identification and quantification were performed using Scaffold (version 5.3.3,
632 Proteome Software), and annotations were derived from PlasmoDB. Proteins were retained for
633 analysis if they had ≥2 unique peptides and valid quantification in at least two replicates.

634

635 **Phosphoproteomic analysis**

636 **Protein Extraction and Digestion via SDS-FASP.** Zygotes of WT and *Pbnek4-ko* lines at 0
637 and 2 hpa were lysed in 400 µl of buffer containing 2% SDS, 25 mM NaCl, 50 mM Tris-HCl
638 (pH 7.4), 2.5 mM EDTA, and 20 mM TCEP, supplemented with a protease and phosphatase
639 inhibitor cocktail (Halt, Thermo Fisher Scientific). Samples were vortexed and heated at 95°C
640 for 10 min with continuous mixing at 400 rpm. Genomic DNA was fragmented using four 10-
641 second sonication pulses at 50% amplitude. Following centrifugation at 17,000 *g* for 30 min,
642 supernatants were collected, and protein concentrations were determined using the Pierce
643 660nm Protein Assay Kit. For alkylation the volume corresponding to 1 mg of protein for each
644 sample was adjusted to 300 µl and then incubated with 48 µl of 0.5 M iodoacetamide for 1 h at
645 room temperature in the dark. Protein digestion was performed using the filter-aided sample
646 preparation (FASP) method with Amicon Ultra-4 30 kDa centrifugal filter units (Millipore).
647 Trypsin (Promega) was added at a 1:80 enzyme-to-protein ratio, and digestion proceeded

648 overnight at room temperature. Resulting peptides were desalted using Pierce Peptide
649 Desalting Spin Columns (Thermo Fisher Scientific) according to the manufacturer's
650 instructions and dried using a speed vacuum concentrator.
651 **TMT-11plex Labelling.** Peptide concentrations were measured using the Pierce Quantitative
652 Colorimetric Peptide Assay (Thermo Fisher Scientific). For each sample, 160 µg of peptides
653 were labelled with 800 µg of TMT reagents (Thermo Fisher Scientific), previously dissolved
654 in 220 µl of 36% acetonitrile and 200 mM EPPS buffer (pH 8.5). Labelling reactions were
655 carried out for 1 h at room temperature and quenched by adding hydroxylamine to a final
656 concentration of 0.3% (v/v). Labelled samples were pooled, desalted using Pierce Peptide
657 Desalting Spin Columns, and dried under vacuum.
658 **Phosphopeptide Enrichment.** Phosphopeptides were enriched using the High-Select Fe-NTA
659 Phosphopeptide Enrichment Kit (Thermo Fisher Scientific) following the manufacturer's
660 protocol. Both the enriched phosphopeptide fractions and the flow-through were desalted using
661 Pierce Peptide Desalting Spin Columns and dried using a speed vacuum concentrator.
662 **LC-MS/MS Analysis.** Dried peptides were reconstituted in 5% acetonitrile with 0.1% formic
663 acid, and 2 µg of each sample was injected into a Vanquish NEO liquid chromatography system
664 (Thermo Fisher Scientific) coupled to an Orbitrap Fusion Lumos Tribrid mass spectrometer
665 (Thermo Fisher Scientific). Peptides were first trapped on an Acclaim PepMap 100 C18 trap
666 column (75 µm × 20 mm, 3 µm particle size) and then separated on a homemade analytical
667 column (75 µm × 500 mm) packed with ReproSil-Pur C18 resin (1.9 µm, 100 Å, Dr. Maisch
668 GmbH). The analytical separation was run for 180 min using a gradient of H_2O/FA 99.9%/0.1%
669 (solvent A) and CH_3CN/H_2O/FA 80.0%/19.9%/0.1% (solvent B). The gradient was run from
670 5 % B to 28 % B in 160 min, then to 40% B in 20 min, then to 99% B in 10 min with a final
671 stay of 20 min at 99 % B. Flow rate was of 250 nL/min an total run time was of 210 min. Data-
672 Dependent Acquisition (DDA) was performed with MS1 full scan at a resolution of 120'000
673 FWHM followed by as many subsequent MS2 scans on selected precursors as possible within
674 3 second maximum cycle time. MS1 was performed in the Orbitrap with an AGC target of
675 $4x10^5$, a maximum injection time of 50 ms and a scan range from 375 to 1500 m/z. MS2 was
676 performed in the Orbitrap at a resolution of 50'000 FWHM using higher-energy collisional
677 dissociation HCD at 38% NCE. Isolation windows was at 0.7 u with an AGC target of $5x10^4$
678 and a maximum injection time of 86 ms. A dynamic exclusion of parent ions of 60 s. with 10
679 ppm mass tolerance was applied.
680 **Data Processing and Analysis.** Raw data files were processed using Proteome Discoverer
681 software version 2.4 (Thermo Fisher Scientific). Spectra were searched against the *P. berghei*

682 ANKA protein database (PlasmoDB.org release 68), the *mus musculus* reference proteome
683 database (UniProt, reviewed, release 2024_06, 17'207 entries) and an in-house database of
684 common contaminants using the Mascot search engine (version 2.6.2, Matrix Science). Search
685 parameters included trypsin as the digestion enzyme with up to one missed cleavage allowed,
686 a precursor mass tolerance of 10 ppm, and a fragment mass tolerance of 0.02 Da.
687 Carbamidomethylation of cysteine (+57.021 Da) and TMT modification of peptide N-termini
688 and lysine residues (+229.163 Da) were set as fixed modifications, while oxidation of
689 methionine (+15.995 Da) and phosphorylation of serine, threonine, and tyrosine (+79.966 Da)
690 were set as variable modifications. Peptide-spectrum matches (PSMs) and peptides were
691 validated using the Percolator algorithm, applying a false discovery rate (FDR) of 1%. Proteins
692 were inferred from the identified peptides and filtered to achieve an FDR of 1%. Quantitative
693 information was extracted using reporter ion intensities from TMT tags, and protein
694 abundances were normalized based on the total peptide amount and scaled across all samples.
695 Protein ratios were calculated using the summed abundances-based approach across groups,
696 and statistical significance was assessed using ANOVA.
697
698 **Data availability**
699 The mass spectrometry proteomics data have been deposited to the ProteomeXchange
700 Consortium via the PRIDE[65] partner repository with the dataset identifier PXD070965 and
701 10.6019/PXD070965 (proteomics and phosphoproteomics) and PXD070161 and
702 10.6019/PXD070161 (GFP immunoprecipitations). RNAseq data have been deposited to the
703 Gene Expression Omnibus under accession number the BioProject ID PRJNA1354107. The
704 authors declare that all other relevant data generated or analysed during this study are included
705 in the article or its supplementary information. Raw data are available for each figure. Materials
706 are available from the corresponding authors on reasonable request.
707
708 **Figure Legends**
709 **Figure 1. NEK4 is located at the MTOC, APC, and nucleus during the early meiotic phase**
710 **of zygote to ookinete development. a.** A schematic diagram of ookinete development showing
711 formation of gametocytes, gametes, and zygote, and the involvement of NEK4 in cellular
712 development and meiosis. The developmental stage and nuclear ploidy (from 1N to 4N) are
713 indicated for each phase. Activation of gametocytes in the mosquito gut initiates sexual
714 development **b.** Live-cell imaging of PbNEK4-GFP location at different time points (hours
715 post-activation, hpa). Green arrowheads indicate the PbNEK4-GFP foci in the nucleus

716 (Hoechst, blue) and at the cell periphery. Insets show magnification of the cell periphery (C)
717 and nucleus (N). The yellow arrowhead indicates the cytoplasmic foci of PbNEK4-GFP. **c.**
718 Schematic summary of the location of PbNEK4-GFP shown in (b), indicating the signal
719 strength in the nucleoplasm, nuclear focus, and at the cell periphery focus over time. **d.**
720 Expansion microscopy of PbNEK4-GFP zygotes at 2 hpa and 4 hpa. The cells were labelled
721 with NHS-ester (gray), anti-GFP antibody (green), and Hoechst (blue). Magnified views of the
722 MTOC and APC regions enclosed by magenta and cyan dashed boxes, respectively, in the
723 whole cell images are shown below. The positions of the MTOC and APC are indicated by
724 magenta and cyan arrows, respectively. **e.** Model illustrating the localisation of NEK4 at the
725 MTOCs, APC and nucleoplasm.
726
727 **Figure 2. NEK4-localised MTOC leads nuclear movement, and directional microtubule**
728 **formation occurs at both the MTOC and the APC during early meiosis. a.** Time-lapse
729 imaging of a PbNEK4-GFP expressing zygote shows nuclear movement. The PbNEK4-GFP
730 foci in the nucleus and at the cell periphery are indicated by magenta and cyan arrowheads,
731 respectively. The lower panel ("Tracing") tracks the position of the PbNEK4-GFP focus (green
732 dot) and the nucleus (blue) over 540 seconds. **b.** Time-lapse imaging of a zygote expressing
733 the microtubule plus-end/MTOC marker PbEB1-GFP (green). The PbEB1-GFP foci in the
734 nucleus and at the cell periphery are indicated by magenta and cyan arrowheads, respectively.
735 The lower panel ("Tracing") tracks the position of the PbEB1-GFP focus (green dot) and the
736 nucleus (blue) over 540 seconds. **c.** Quantification of the percentage of zygotes showing
737 nuclear movement at 0, 2, 4, and 6 hpa. Data are mean ± SEM from three independent
738 experiments. Black dots show the result from each experiment. **d.** Schematic model of nuclear
739 movement, illustrating the association of NEK4/EB1 foci with the moving nucleus at 2-4 hpa.
740 **e.** Expansion microscopy showing microtubule organisation in developing zygotes.
741 Microtubules (α-tubulin, green) are shown at 2 hpa with either one or two MTOCs, and at 4
742 hpa with separated MTOCs. Magnified views of the MTOC and APC regions enclosed by
743 magenta and cyan dashed boxes, respectively, in the whole cell images are shown below. The
744 positions of the MTOC and APC are indicated by magenta and cyan arrows, respectively. **f.**
745 Model of the microtubule organisation in a developing zygote, illustrating the formation of
746 perinuclear and APC microtubules and the location of PbNEK4-GFP at the MTOCs, APC and
747 nucleoplasm.
748

749 **Figure 3. NEK4 is essential for DNA replication, nuclear migration, microtubule**
750 **formation, and morphological transformation from zygote to ookinete. a.** Live-cell
751 imaging of control (PbNEK4-GFP) and *Pbnek4-ko* parasites from 2 to 20 hpa. Unlike the
752 control which develops into an elongated ookinete, *Pbnek4-ko* parasites remain round and fail
753 to develop. **b.** Quantification of nuclear movement in control (PbNEK4-GFP, blue) and
754 *Pbnek4-ko* (gray) zygotes at 2- and 4 hpa. Nuclear movement is significantly reduced in the
755 *Pbnek4-ko* mutant both at 2- and 4 hpa. Data are mean ± SEM from three independent
756 experiments. Black dots show the result from each experiment. P-values were determined by
757 Welch's t-test. **c.** Expansion microscopy comparing microtubule organisation (α-tubulin,
758 green) in WT and *Pbnek4-ko* zygotes at 2 and 4 hpa. Magnified views of the MTOC and APC
759 regions enclosed by magenta and cyan dashed boxes, respectively, in the whole cell images are
760 shown below. The positions of the MTOC and APC are indicated by magenta and cyan arrows,
761 respectively. *Pbnek4-ko* zygotes show a single MTOC and disrupted microtubule formation, in
762 contrast to the well-organised perinuclear and APC microtubules in WT zygotes. **d.** Schematic
763 model summarising the defects in *Pbnek4-ko* zygotes, including the persistence of a single
764 MTOC, disrupted microtubule formation, and reduced nuclear movement.
765
766 **Figure 4. Electron microscopy shows that cytoskeletal development and condensed**
767 **chromosome formation during early meiosis are blocked in *Pbnek4-ko* zygotes. a.** TEM
768 images of WT and *Pbnek4-ko* zygotes at 2 hpa (panels 1-8) and 4 hpa (panels 9-18). N, nucleus;
769 APC, apical polar complex; APR, Apical polar ring; A-Mt, APC microtubule; Pn-Mt,
770 perinuclear microtubule; NM, nuclear membrane. Magenta arrowheads show condensed
771 chromosomes. **b.** Slice images of WT and *Pbnek4-ko* zygotes at 4 hpa, obtained by SBF-SEM.
772 The whole-cell view shows the development of the APC in the WT zygote. The magnified
773 views of the nucleus show the presence of thread-like condensed chromosomes (magenta
774 arrowheads) and the formation of potential synaptonemal complexes (cyan arrowheads), where
775 these condensed chromosomes form pairs via a central linear structure. The insets show
776 magnified views of a thread-like condensed chromosomes and synaptonemal complex. These
777 developmental features were completely absent in *Pbnek4-ko* zygotes. **c.** Quantification of the
778 percentage of cells with a developing APC and condensed chromosomes in WT and *Pbnek4-*
779 *ko* zygotes at 4 hpa, based on three independent SBF-SEM datasets. Data are shown as mean
780 ± SEM, with black dots representing the results from each dataset. **d.** 3D models of WT and
781 *Pbnek4-ko* zygotes at 4 hpa, reconstructed from SBF-SEM datasets. The WT model illustrates

782 the developed APC (orange) with APR (gray), the presence of condensed, thread-like
783 chromosomes within the nucleus (blue; some of which are attached to the nuclear envelope),
784 and the separating MTOCs (purple). In contrast, the *Pbnek4-ko* zygote model shows that none
785 of these developmental events have occurred.
786
787 **Figure 5. Global transcriptomic, proteomics and phosphoproteomic analysis reveals**
788 **NEK4-dependent transcriptional and phosphorylation events during *Plasmodium* zygote**
789 **activation. a.** Volcano plot showing differentially expressed transcripts in *Pbnek4-ko* parasites
790 compared to WT controls at 2 hpa (RNA-seq). The $\log_2$ fold change (FC) is plotted against -
791 $\log_{10}$(adjusted p-value). Red and blue dots indicate significantly upregulated and
792 downregulated genes, respectively. *NEK4* and key meiotic genes that are significantly
793 downregulated in *Pbnek4-ko* at 2 hpa are highlighted with yellow dots and gene names. Dotted
794 lines indicate the threshold for statistical significance (adjusted p-value ≤ 0.05 and fold change
795 ≥ 1.5). The underlying data are provided in Supplementary Table 1. **b.** Gene Ontology (GO)
796 analysis of differentially expressed transcripts by RNA-seq in *Pbnek4-ko* versus WT zygotes
797 at 2 hpa. Genes in each term are listed in Supplementary Table 2. The analysis was performed
798 using GO slim terms in PlasmoDB. BP = Biological Process; CC = Cellular component; MF =
799 Molecular Function. **c**. Table displaying selected proteins, corresponding gene ID and
800 representation by the number of peptides from the proteins identified in a GFP-trap pulldown
801 assay with precipitates of either PbNEK4-GFP or WT-GFP zygotes at 2 hpa. **d-g.** Volcano
802 plots displaying changes in total protein and phosphopeptide abundance. The $\log_2$ fold change
803 (derived from the average of three biological replicates each) is plotted against the -$\log_{10}$ p-
804 value. The dotted lines indicate the threshold for statistical significance (p-value ≤ 0.05 and
805 fold change ≥ 1.5). Significantly upregulated and downregulated proteins/phosphopeptides are
806 shown as red and blue dots, respectively. Proteins/phosphopeptides with non-significant
807 changes are shown as grey dots. **d.** Comparison of protein abundance between WT gametocytes
808 at 0 hpa and WT zygotes at 2 hpa. **e.** Comparison of protein abundance between *Pbnek4-ko*
809 and WT zygotes at 2 hpa. **f.** Comparison of phosphopeptide abundance between WT
810 gametocytes at 0 hpa and WT zygotes at 2 hpa. **g.** Comparison of phosphopeptide abundance
811 between *Pbnek4-ko* and WT zygotes at 2 hpa. Key phosphopeptides from proteins of interest
812 that are significantly upregulated in WT at 2 hpa (f) and downregulated in the *Pbnek4-ko*
813 mutant at 2 hpa (g) are highlighted with yellow dots and protein names. **h-i.** GO analysis of
814 differentially abundant phosphopeptides in WT zygotes at 2 hpa versus 0 hpa (h) and *Pbnek4-*

815 *ko* versus WT zygotes at 2 hpa (i). Genes in each term are listed in Supplementary Table 8 and
816 10. The analysis was performed using GO slim terms in PlasmoDB. **e.** Summary table
817 displaying selected proteins with significant changes in phosphopeptide abundance from the
818 phosphoproteomics screen. The $\log_2$ fold change ($\log_2$FC) values of identified phosphopeptides
819 are represented by a colour gradient from red (decrease) to blue (increase). Significant log2FC
820 values (p-value ≤ 0.05) are shown in black text, while non-significant values are in gray.
821 Corresponding phosphopeptide sequences are also listed.
822
823 **Figure 6. *Plasmodium* NEK4 acts as a key regulator driving the early events of meiosis.** A
824 model illustrating the central function of NEK4 in coordinating key developmental processes
825 during the zygote-to-ookinete development. The top panel shows the canonical meiotic stages
826 in the model organism *Schizosaccharomyces pombe* (*S. pombe*) for comparison. The middle
827 panel depicts the predicted steps and timing of meiosis in *Plasmodium* from zygote formation,
828 meiosis I to meiosis II, based on previous observations. In *Pbnek4-ko* mutants, DNA replication
829 is impaired, blocking progression to meiotic prophase. In *S. pombe*, active nuclear movement,
830 known as horsetail nuclear movement, occurs during prophase, followed by chromosome
831 pairing and crossover mediated by linear elements (LinEs). In contrast, our observations in
832 *Plasmodium* suggest that between 2 and 4 hpa, active nuclear movement similar to the horsetail
833 movement occurs concurrently with the formation of structures resembling synaptonemal
834 complexes between condensed chromosomes. The bottom panel proposes that NEK4 regulates
835 four crucial modules: (1) MTOC/Microtubule dynamics (e.g. MARK/MELK, PI3K/PI4K), (2)
836 Meiosis-specific proteins (e.g. Rec8, HOP1), (3) Sexual development factors (e.g., FD2, AP2-
837 O), (4) DNA/chromosome functions (e.g. RCC, POLD3). Through these pathways, NEK4
838 orchestrates MTOC separation, microtubule formation at MTOC and APC, DNA replication,
839 and chromosome condensation, which are all essential for successful meiosis and subsequent
840 ookinete development. Based on the function of perinuclear microtubules in other eukaryotes
841 during meiosis, the perinuclear microtubules observed in *Plasmodium* zygotes are likely
842 associated with nuclear movement or intranuclear chromosome movement. We predict that
843 effectors such as cytoplasmic dynein and Sun1 mediate these functions.
844
845 **Extended Data Fig. legend**
846 **Extended Data Fig. 1. *Plasmodium* NEK phylogeny, domain structure, function, and**
847 **generation of PbNEK-GFP parasites. a.** Phylogenetic tree of NIMA-related protein kinases

848 (NEKs) from *Plasmodium berghei* (Pb, light blue; PbNEK4, blue), *Plasmodium falciparum*
849 (Pf, red), *Homo sapiens* (Hs, green), including NIMA (black) from *Aspergillus nidulans*. **b.**
850 Domain structures of PbNEKs. **c.** Summary table of the function, expression stage, and
851 localisation of PbNEKs. **d.** Schematic representation of the endogenous *nek4* locus, the GFP-
852 tagging construct, and the recombined *nek4* locus following single homologous recombination.
853 Arrows indicate the position of PCR primers used to confirm successful integration of the
854 construct. **e.** Diagnostic PCR of *nek4* and WT-GFP parasites using the diagnostic primers to
855 show the correct integration. Integration of the *nek4* tagging construct gives a band of ~1400
856 bp. **f.** Western blot showing the expression of endogenous PbNEK4-GFP detected by anti-GFP
857 antibody. The positions corresponding to the molecular weights of GFP (~27 kDa) and
858 PbNEK4-GFP (~74 kDa) are indicated by arrows, respectively.
859
860 **Extended Data Fig. 2. PbNEK4-GFP localisation dynamics during zygote-ookinete**
861 **development.** Live-cell imaging of PbNEK4-GFP location at different time points (minutes or
862 hours post-activation, mpa or hpa). PbNEK4-GFP (green) parasites were labelled with Hoechst
863 (blue) and 13.1 antibody, which recognises P28 protein on the surface of zygotes and ookinetes.
864
865 **Extended Data Fig. 3. Expansion microscopy comparing microtubule organisation in**
866 **non-activated WT and *Pbnek4-ko* female gametocytes and WT zygotes at 2 hpa. a, b.**
867 NHS-ester staining (gray) revealed that the apical polar complex (APC) had not yet in both WT
868 (a) and *Pbnek4-ko* (b) female gametocytes before activation. A structure presumed to be the
869 MTOC was also visible (magenta arrowhead), although it appeared smaller compared to that
870 in zygotes at 2 hpa. Furthermore, anti α-tubulin antibody (green) and Hoechst (blue) staining
871 revealed that no microtubule formation was observed around the potential MTOC and nucleus.
872 **c.** In contrast, zygotes activated for 2 hours displayed the development of the APC and MTOCs,
873 along with microtubule structures extending form them.
874
875 **Extended Data Fig. 4. Generation and genotypic analysis of *Pbnek4-ko* parasites. a.**
876 Schematic representation of the endogenous *nek4* locus, the targeting knockout construct and
877 the recombined *nek4* locus following double homologous crossover recombination. Arrows P1
878 and P2 indicate PCR primers used to confirm successful integration in the *nek4* locus following
879 recombination, and arrows P3, 4, 5 and 6 indicate PCR primers used to show deletion of the

880 *nek4* gene. **b.** Integration PCR of the *nek4* locus in WT and *Pbnek4-ko* parasites using the
881 primers, P1-6.
882
883 **Extended Data Fig. 5. qRT-PCR analysis of *Pbnek4-ko* and WT zygotes at 2 hpa and**
884 **proteomic and phosphoproteomic analysis of *Pbnek4-ko* and WT zygotes at 0 hpa and**
885 ***Pbnek4-ko* gametocytes at 0 hpa and *Pbnek4-ko* zygotes at 2 hpa. c.** Expression level
886 validation of *nek4* and meiotic related genes using qRT-PCR in *Pbnek4-ko* and WT zygotes at
887 2 hpa. Shown is mean ± SEM; n = 3 independent experiments. Multiple comparisons *t* test,
888 with post hoc test of Holm–Sidak showed significant differences in relative expression.
889 *adjusted p-value < 0.05, **adjusted p-value < 0.01. **b-e.** Volcano plots displaying changes in
890 total protein and phosphopeptide abundance between *Pbnek4-ko* and WT zygotes at 0 hpa and
891 between *Pbnek4-ko* gametocytes at 0 hpa and *Pbnek4-ko* zygotes at 2 hpa. The $\log_2$ fold change
892 (derived from the average of three biological replicates each) is plotted against the $-\log_{10}$ p-
893 value. The dotted lines indicate the threshold for statistical significance (p-value ≤ 0.05 and
894 fold change ≥ 1.5). Significantly upregulated and downregulated proteins/phosphopeptides are
895 shown as red and blue dots, respectively. Proteins/phosphopeptides with non-significant
896 changes are shown as grey dots. **b.** Comparison of protein abundance between *Pbnek4-ko* and
897 WT zygotes at 0 hpa. **c.** Comparison of protein abundance between *Pbnek4-ko* gametocytes at
898 0 hpa and *Pbnek4-ko* zygotes at 2 hpa. **d.** Comparison of phosphopeptide abundance between
899 *Pbnek4-ko* and WT zygotes at 0 hpa. **e.** Comparison of phosphopeptide abundance between
900 *Pbnek4-ko* gametocytes at 0 hpa and *Pbnek4-ko* zygotes at 2 hpa. Key phosphopeptides from
901 proteins of interest that are significantly upregulated in WT at 2 hpa (f) and downregulated in
902 the *Pbnek4-ko* mutant at 2 hpa (g) are highlighted with yellow dots and protein names.
903
904 **Supplementary Table 1: RNA-Seq data analysis of *Pbnek4-ko* vs WT parasite 2 hpa**
905 **Supplementary Table 2: Gene Ontology Analysis of RNA-Seq data**
906 **Supplementary Table 3: Quantitative proteomics of WT 2 hpa versus WT 0 hpa parasites**
907 **Supplementary Table 4: Quantitative proteomics of *Pbnek4-ko* 2 hpa versus WT 2 hpa**
908 **parasites**
909 **Supplementary Table 5: Quantitative proteomics of *Pbnek4-ko* 0 hpa versus WT 0 hpa**
910 **parasites**
911 **Supplementary Table 6: Quantitative proteomics of *Pbnek4-ko* 2 hpa versus *Pbnek4-ko* 0**
912 **hpa parasites**

913 **Supplementary Table 7: Quantitative phosphoproteomics of WT 2 hpa versus WT 0 hpa**
914 **parasites**
915 **Supplementary Table 8: Gene Ontology Analysis of phosphoproteomic data for WT 2**
916 **hpa versus WT 0 hpa parasites**
917 **Supplementary Table 9: Quantitative phosphoproteomics of *Pbnek4-ko* 2 hpa versus WT**
918 **2 hpa parasites**
919 **Supplementary Table 10: Gene Ontology Analysis of phosphoproteomic data for *Pbnek4-***
920 ***ko* 2 hpa versus WT 2 hpa parasites**
921 **Supplementary Table 11: Quantitative phosphoproteomics of *Pbnek4-ko* 2 hpa versus**
922 ***Pbnek4-ko* 0 hpa parasites**
923 **Supp. Table 12: Quantitative phosphoproteomics of *Pbnek4-ko* 0 hpa versus WT 0 hpa**
924 **parasites**
925 **Supplementary Table 13: GFP-Trap downs of PbNEK4-GFP parasites 2 hpa**
926 **Supplementary Table 14: Primers used in this study**
927
928 **Supplementary Video 1**
929 Time-lapse video microscopy of nuclear movement in the Hoechst (blue)-stained PbNEK4-
930 GFP (green) zygotes at 2 hpa. Video is played back at 50× speed. Scale bar = 5 μm.
931
932 **Supplementary Video 2**
933 Time-lapse video microscopy of nuclear movement in the single zygote from Supplementary
934 Video 1 (blue; Hoechst, green; PbNEK4-GFP). Video is played back at 50× speed. Scale bar =
935 5 μm.
936
937 **Supplementary Video 3**
938 Time-lapse video microscopy of nuclear movement in the Hoechst (blue)-stained PbEB1-GFP
939 (green) zygotes at 2 hpa. Video is played back at 50× speed. Scale bar = 5 μm.
940
941 **Supplementary Video 4**
942 Time-lapse video microscopy of nuclear movement in the single zygote from Supplementary
943 Video 1 (blue; Hoechst, green; PbEB1-GFP). Video is played back at 50× speed. Scale bar = 5
944 μm.
945

Acknowledgements

RT and MH are supported by an ERC advance grant funded by UKRI Frontier Science (EP/X024776/1), MRC UK (MR/K011782/1), and BBSRC (BB/L013827/1, BB/X014681/1). MZ and DB were supported as research fellows (EP/X024776/1). RY and DSG are supported by the BBSRC (BB/X014681/1). AAH is supported by the Francis Crick Institute (FC001097), which receives core funding from the Cancer Research UK (FC001097), the UK Medical Research Council (FC001097), and the Wellcome Trust (FC001097). KGLR is supported by the NIH/NIAID (R01 AI136511) and the University of California, Riverside NIFA-Hatch-225935. ECT was supported by a personal fellowship from the Nederlandse Organisatie voor Wetenschappelijk Onderzoek (NWO), the Netherlands (grant no. VI. Veni.202.223). We thank the School of Life Sciences Imaging (SLIM) for providing access to confocal and SIM microscopy and Dr Robert Markus for technical assistance. We thank the Nanoscale and Microscale Research Centre (nmRC) for providing access to instrumentation and Dr Michael W. Fey, Dr Julie Watts and Ms Nicola J. Weston for technical assistance. For Open Access, the authors have applied a CC BY public copyright licence to any Author Accepted Manuscript version arising from this submission. We thank Cleidiane Zampronio at Warwick University for mass spectrometry methods and Bio Support Unit, University of Nottingham for maintenance of mice used in this study.

References

1. Bolcun-Filas E, Handel MA. Meiosis: the chromosomal foundation of reproduction. *Biol Reprod* **99**, 112-126 (2018).

2. Marston AL, Amon A. Meiosis: cell-cycle controls shuffle and deal. *Nat Rev Mol Cell Biol* **5**, 983-997 (2004).

3. Ohkura H. Meiosis: an overview of key differences from mitosis. *Cold Spring Harb Perspect Biol* **7**, (2015).

4. Pesin JA, Orr-Weaver TL. Regulation of APC/C activators in mitosis and meiosis. *Annu Rev Cell Dev Biol* **24**, 475-499 (2008).

5. Pereira C, Smolka MB, Weiss RS, Brieno-Enriquez MA. ATR signaling in mammalian meiosis: From upstream scaffolds to downstream signaling. *Environ Mol Mutagen* **61**, 752-766 (2020).

6. Loidl J. Conservation and Variability of Meiosis Across the Eukaryotes. *Annu Rev Genet* **50**, 293-316 (2016).

7. Mirzaghaderi G, Horandl E. The evolution of meiotic sex and its alternatives. *Proc Biol Sci* **283**, (2016).

8. Guttery DS, Zeeshan M, Holder AA, Tromer EC, Tewari R. Meiosis in Plasmodium: how does it work? *Trends Parasitol* **39**, 812-821 (2023).

9. Guttery DS, Zeeshan M, Ferguson DJP, Holder AA, Tewari R. Division and Transmission: Malaria Parasite Development in the Mosquito. *Annu Rev Microbiol* **76**, 113-134 (2022).

10. WHO. World malaria report 2024. *World Health Organisation* **ISBN 978-992-974-010444-010440**, (2024).

11. Sinden RE. Gametocytogenesis in Plasmodium spp., and observations on the meiotic division. *Ann Soc Belg Med Trop* **65 Suppl 2**, 21-33 (1985).

12. Sinden RE, Canning EU, Spain B. Gametogenesis and fertilization in Plasmodium yoelii nigeriensis: a transmission electron microscope study. *Proc R Soc Lond B Biol Sci* **193**, 55-76 (1976).

13. Zeeshan M*, et al.* Real-time dynamics of Plasmodium NDC80 reveals unusual modes of chromosome segregation during parasite proliferation. *J Cell Sci* **134**, (2020).

14. Guttery DS*, et al.* Genome-wide functional analysis of Plasmodium protein phosphatases reveals key regulators of parasite development and differentiation. *Cell Host Microbe* **16**, 128-140 (2014).

15. Tewari R*, et al.* The systematic functional analysis of Plasmodium protein kinases identifies essential regulators of mosquito transmission. *Cell Host Microbe* **8**, 377-387 (2010).

16. Ward P, Equinet L, Packer J, Doerig C. Protein kinases of the human malaria parasite Plasmodium falciparum: the kinome of a divergent eukaryote. *BMC Genomics* **5**, 79 (2004).

17. Gao H*, et al.* ISP1-Anchored Polarization of GCbeta/CDC50A Complex Initiates Malaria Ookinete Gliding Motility. *Curr Biol* **28**, 2763-2776 e2766 (2018).

18. Fry AM, Bayliss R, Roig J. Mitotic Regulation by NEK Kinase Networks. *Front Cell Dev Biol* **5**, 102 (2017).

19. Fry AM, O'Regan L, Sabir SR, Bayliss R. Cell cycle regulation by the NEK family of protein kinases. *J Cell Sci* **125**, 4423-4433 (2012).

1028 20. Brieno-Enriquez MA, Moak SL, Holloway JK, Cohen PE. NIMA-related kinase 1 (NEK1)
1029 regulates meiosis I spindle assembly by altering the balance between alpha-Adducin and
1030 Myosin X. *PLoS One* **12**, e0185780 (2017).

1031
1032 21. Reininger L*, et al.* A NIMA-related protein kinase is essential for completion of the sexual
1033 cycle of malaria parasites. *J Biol Chem* **280**, 31957-31964 (2005).

1034
1035 22. Reininger L, Garcia M, Tomlins A, Muller S, Doerig C. The Plasmodium falciparum, Nima-
1036 related kinase Pfnek-4: a marker for asexual parasites committed to sexual differentiation.
1037 *Malar J* **11**, 250 (2012).

1038
1039 23. Reininger L*, et al.* An essential role for the Plasmodium Nek-2 Nima-related protein kinase in
1040 the sexual development of malaria parasites. *J Biol Chem* **284**, 20858-20868 (2009).

1041
1042 24. Zeeshan M*, et al.* Plasmodium NEK1 coordinates MTOC organisation and kinetochore
1043 attachment during rapid mitosis in male gamete formation. *PLoS Biol* **22**, e3002802 (2024).

1044
1045 25. Cromer L*, et al.* Rapid meiotic prophase chromosome movements in Arabidopsis thaliana are
1046 linked to essential reorganization at the nuclear envelope. *Nat Commun* **15**, 5964 (2024).

1047
1048 26. Christophorou N, Rubin T, Bonnet I, Piolot T, Arnaud M, Huynh JR. Microtubule-driven
1049 nuclear rotations promote meiotic chromosome dynamics. *Nat Cell Biol* **17**, 1388-1400 (2015).

1050
1051 27. Saito TT, Tougan T, Okuzaki D, Kasama T, Nojima H. Mcp6, a meiosis-specific coiled-coil
1052 protein of Schizosaccharomyces pombe, localizes to the spindle pole body and is required for
1053 horsetail movement and recombination. *J Cell Sci* **118**, 447-459 (2005).

1054
1055 28. Ding DQ, Chikashige Y, Haraguchi T, Hiraoka Y. Oscillatory nuclear movement in fission
1056 yeast meiotic prophase is driven by astral microtubules, as revealed by continuous observation
1057 of chromosomes and microtubules in living cells. *J Cell Sci* **111 (Pt 6)**, 701-712 (1998).

1058
1059 29. Yamamoto A, West RR, McIntosh JR, Hiraoka Y. A cytoplasmic dynein heavy chain is
1060 required for oscillatory nuclear movement of meiotic prophase and efficient meiotic
1061 recombination in fission yeast. *J Cell Biol* **145**, 1233-1249 (1999).

1062
1063 30. Vogel SK, Pavin N, Maghelli N, Julicher F, Tolic-Norrelykke IM. Self-organization of dynein
1064 motors generates meiotic nuclear oscillations. *PLoS Biol* **7**, e1000087 (2009).

1065
1066 31. Zeeshan M*, et al.* Plasmodium ARK2 and EB1 drive unconventional spindle dynamics, during
1067 chromosome segregation in sexual transmission stages. *Nat Commun* **14**, 5652 (2023).

1068
1069 32. Yang S*, et al.* EB1 decoration of microtubule lattice facilitates spindle-kinetochore lateral
1070 attachment in Plasmodium male gametogenesis. *Nat Commun* **14**, 2864 (2023).

1071
1072 33. Chikashige Y*, et al.* Telomere-led premeiotic chromosome movement in fission yeast. *Science*
1073 **264**, 270-273 (1994).

34. Labella S, Woglar A, Jantsch V, Zetka M. Polo kinases establish links between meiotic chromosomes and cytoskeletal forces essential for homolog pairing. *Dev Cell* **21**, 948-958 (2011).

35. Hirai M, Maeta A, Mori T, Mita T. Pb103 Regulates Zygote/Ookinete Development in Plasmodium berghei via Double Zinc Finger Domains. *Pathogens* **10**, (2021).

36. Nishi T, Kaneko I, Iwanaga S, Yuda M. Identification of a novel AP2 transcription factor in zygotes with an essential role in Plasmodium ookinete development. *PLoS Pathog* **18**, e1010510 (2022).

37. Mlambo G, Coppens I, Kumar N. Aberrant sporogonic development of Dmc1 (a meiotic recombinase) deficient Plasmodium berghei parasites. *PLoS One* **7**, e52480 (2012).

38. Yuda M, Kaneko I, Murata Y, Iwanaga S, Nishi T. Mechanisms of triggering malaria gametocytogenesis by AP2-G. *Parasitol Int* **84**, 102403 (2021).

39. Modrzynska K*, et al.* A Knockout Screen of ApiAP2 Genes Reveals Networks of Interacting Transcriptional Regulators Controlling the Plasmodium Life Cycle. *Cell Host Microbe* **21**, 11-22 (2017).

40. Russell AJC*, et al.* Regulators of male and female sexual development are critical for the transmission of a malaria parasite. *Cell Host Microbe* **31**, 305-319 e310 (2023).

41. Kaneko I, Nishi T, Iwanaga S, Yuda M. Differentiation of Plasmodium male gametocytes is initiated by the recruitment of a chromatin remodeler to a male-specific cis-element. *Proc Natl Acad Sci U S A* **120**, e2303432120 (2023).

42. Hart KJ, Power BJ, Rios KT, Sebastian A, Lindner SE. The Plasmodium NOT1-G paralogue is an essential regulator of sexual stage maturation and parasite transmission. *PLoS Biol* **19**, e3001434 (2021).

43. Drewes G, Ebneth A, Preuss U, Mandelkow EM, Mandelkow E. MARK, a novel family of protein kinases that phosphorylate microtubule-associated proteins and trigger microtubule disruption. *Cell* **89**, 297-308 (1997).

44. Cao LS, Wang J, Chen Y, Deng H, Wang ZX, Wu JW. Structural basis for the regulation of maternal embryonic leucine zipper kinase. *PLoS One* **8**, e70031 (2013).

45. Liu B, Liu C, Li Z, Liu W, Cui H, Yuan J. A subpellicular microtubule dynein transport machinery regulates ookinete morphogenesis for mosquito transmission of Plasmodium yoelii. *Nat Commun* **15**, 8590 (2024).

46. Grallert A, Hagan IM. Schizosaccharomyces pombe NIMA-related kinase, Fin1, regulates spindle formation and an affinity of Polo for the SPB. *EMBO J* **21**, 3096-3107 (2002).

47. Grallert A, Krapp A, Bagley S, Simanis V, Hagan IM. Recruitment of NIMA kinase shows that maturation of the S. pombe spindle-pole body occurs over consecutive cell cycles and reveals a role for NIMA in modulating SIN activity. *Genes Dev* **18**, 1007-1021 (2004).

48. Zalli D, Bayliss R, Fry AM. The Nek8 protein kinase, mutated in the human cystic kidney disease nephronophthisis, is both activated and degraded during ciliogenesis. *Hum Mol Genet* **21**, 1155-1171 (2012).

49. Koch LB, Spanos C, Kelly V, Ly T, Marston AL. Rewiring of the phosphoproteome executes two meiotic divisions in budding yeast. *EMBO J* **43**, 1351-1383 (2024).

50. Sivakova B*, et al.* Quantitative proteomics and phosphoproteomics profiling of meiotic divisions in the fission yeast Schizosaccharomyces pombe. *Sci Rep* **14**, 23105 (2024).

51. Anderson-White B, Beck JR, Chen CT, Meissner M, Bradley PJ, Gubbels MJ. Cytoskeleton assembly in Toxoplasma gondii cell division. *Int Rev Cell Mol Biol* **298**, 1-31 (2012).

52. Tosetti N*, et al.* Essential function of the alveolin network in the subpellicular microtubules and conoid assembly in Toxoplasma gondii. *Elife* **9**, (2020).

53. Harding CR, Frischknecht F. The Riveting Cellular Structures of Apicomplexan Parasites. *Trends Parasitol* **36**, 979-991 (2020).

54. Burrell A*, et al.* Cellular electron tomography of the apical complex in the apicomplexan parasite Eimeria tenella shows a highly organised gateway for regulated secretion. *PLoS Pathog* **18**, e1010666 (2022).

55. Chen CT, Gubbels MJ. TgCep250 is dynamically processed through the division cycle and is essential for structural integrity of the Toxoplasma centrosome. *Mol Biol Cell* **30**, 1160-1169 (2019).

56. Hu X, O'Shaughnessy WJ, Beraki TG, Reese ML. Loss of the Conserved Alveolate Kinase MAPK2 Decouples Toxoplasma Cell Growth from Cell Division. *mBio* **11**, (2020).

57. Guttery DS*, et al.* A unique protein phosphatase with kelch-like domains (PPKL) in Plasmodium modulates ookinete differentiation, motility and invasion. *PLoS Pathog* **8**, e1002948 (2012).

58. Mytlis A, Levy K, Elkouby YM. The many faces of the bouquet centrosome MTOC in meiosis and germ cell development. *Curr Opin Cell Biol* **81**, 102158 (2023).

59. Zeeshan M*, et al.* A novel SUN1-ALLAN complex coordinates segregation of the bipartite MTOC across the nuclear envelope during rapid closed mitosis in Plasmodium berghei. *Elife* **14**, (2025).

60. Janse CJ, *et al.* High efficiency transfection of Plasmodium berghei facilitates novel selection procedures. *Mol Biochem Parasitol* **145**, 60-70 (2006).

61. Ferguson DJ, *et al.* Maternal inheritance and stage-specific variation of the apicoplast in Toxoplasma gondii during development in the intermediate and definitive host. *Eukaryot Cell* **4**, 814-826 (2005).

62. Hair M, Moreira-Leite F, Ferguson DJP, Zeeshan M, Tewari R, Vaughan S. Atypical flagella assembly and haploid genome coiling during male gamete formation in Plasmodium. *Nat Commun* **14**, 8263 (2023).

63. Yanase R, *et al.* Divergent Plasmodium kinases drive MTOC, kinetochore and axoneme organisation in male gametogenesis. *Life Sci Alliance* **8**, (2025).

64. Liffner B, Silva T, Vega-Rodriguez J, Absalon S. Mosquito Tissue Ultrastructure-Expansion Microscopy (MoTissU-ExM) enables ultrastructural and anatomical analysis of malaria parasites and their mosquito. *BMC Mehods* **1**, (2024).

65. Perez-Riverol Y, *et al.* The PRIDE database at 20 years: 2025 update. *Nucleic Acids Res* **53**, D543-D553 (2025).

Figure 1

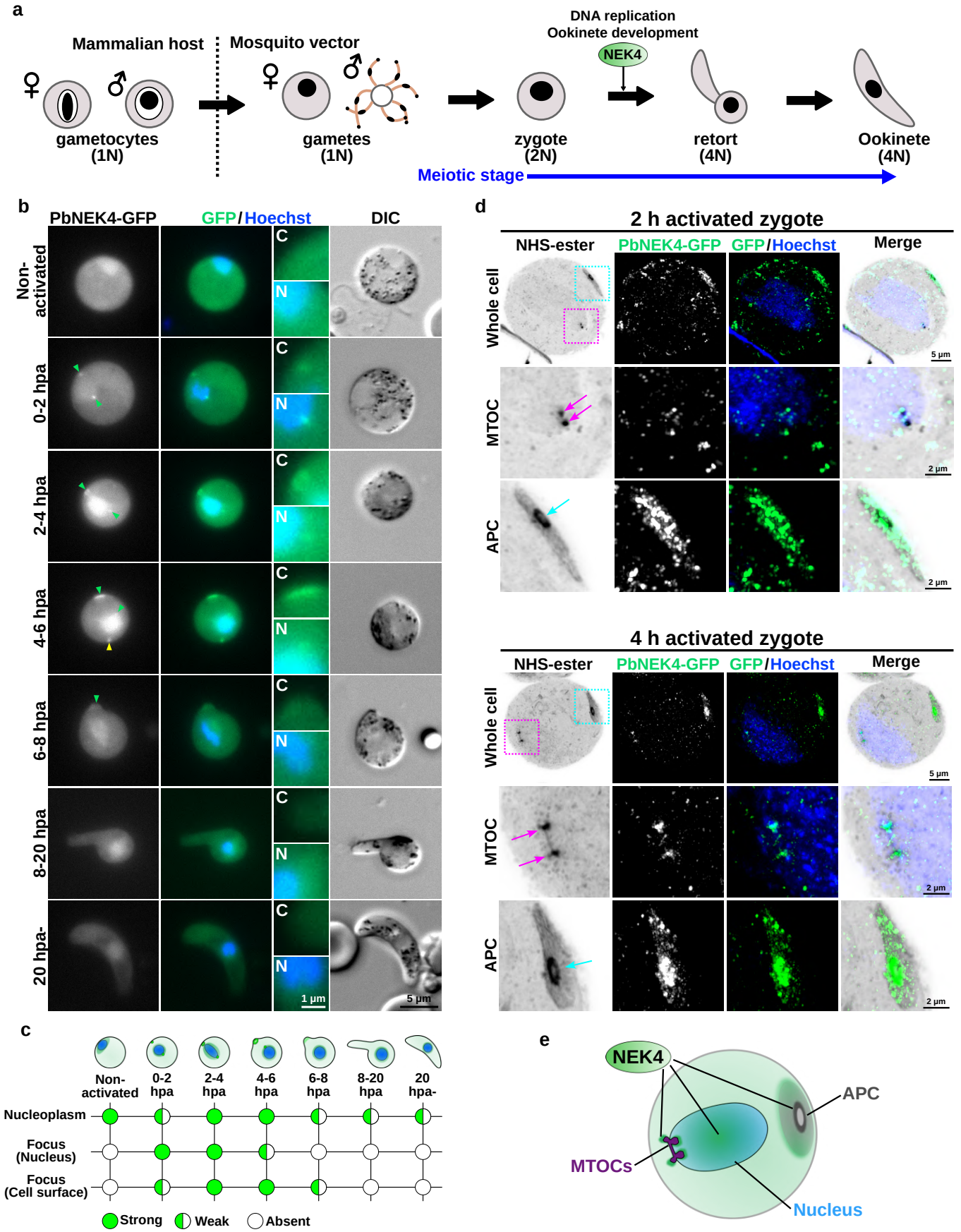
a
Mammalian host
Mosquito vector
DNA replication
Ookinete development
NEK4
gametocytes (1N)
gametes (1N)
zygote (2N)
retort (4N)
Ookinete (4N)
Meiotic stage
b
PbNEK4-GFP
GFP/Hoechst
DIC
Non-activated
0-2 hpa
2-4 hpa
4-6 hpa
6-8 hpa
8-20 hpa
20 hpa-
C
N
1 µm
5 µm
c
Non-activated
0-2 hpa
2-4 hpa
4-6 hpa
6-8 hpa
8-20 hpa
20 hpa-
Nucleoplasm
Focus (Nucleus)
Focus (Cell surface)
Strong
Weak
Absent
d
2 h activated zygote
4 h activated zygote
NHS-ester
PbNEK4-GFP
GFP/Hoechst
Merge
Whole cell
MTOC
APC
5 µm
2 µm
e
NEK4
APC
MTOCs
Nucleus

Figure 2

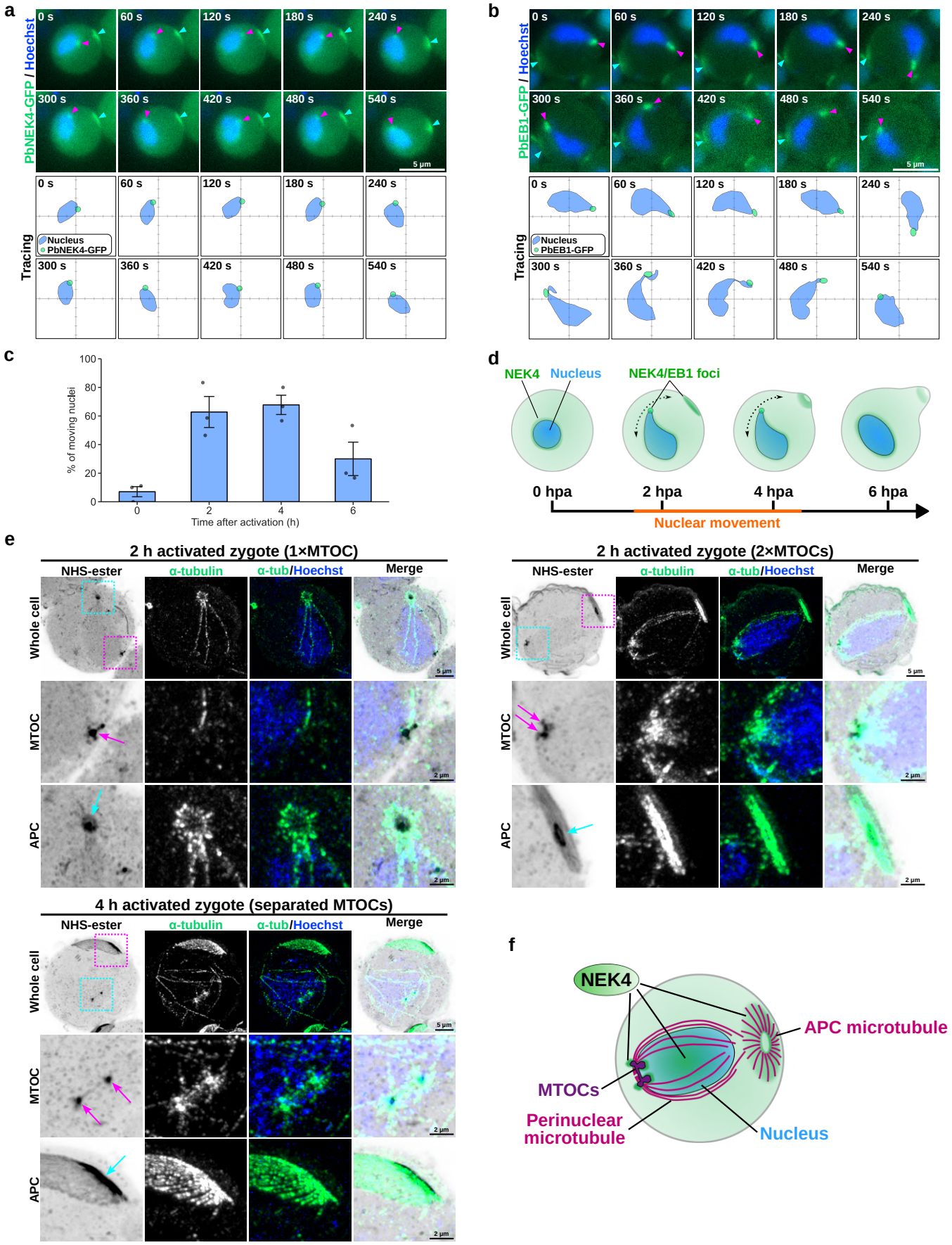
a
PbNEK4-GFP / Hoechst
0 s
60 s
120 s
180 s
240 s
300 s
360 s
420 s
480 s
540 s
5 µm
Tracing
Nucleus
PbNEK4-GFP
b
PbEB1-GFP / Hoechst
PbEB1-GFP
c
% of moving nuclei
Time after activation (h)
d
NEK4
Nucleus
NEK4/EB1 foci
0 hpa
2 hpa
4 hpa
6 hpa
Nuclear movement
e
2 h activated zygote (1×MTOC)
2 h activated zygote (2×MTOCs)
4 h activated zygote (separated MTOCs)
NHS-ester
α-tubulin
α-tub/Hoechst
Merge
Whole cell
MTOC
APC
f
NEK4
APC microtubule
MTOCs
Perinuclear microtubule
Nucleus

Figure 3

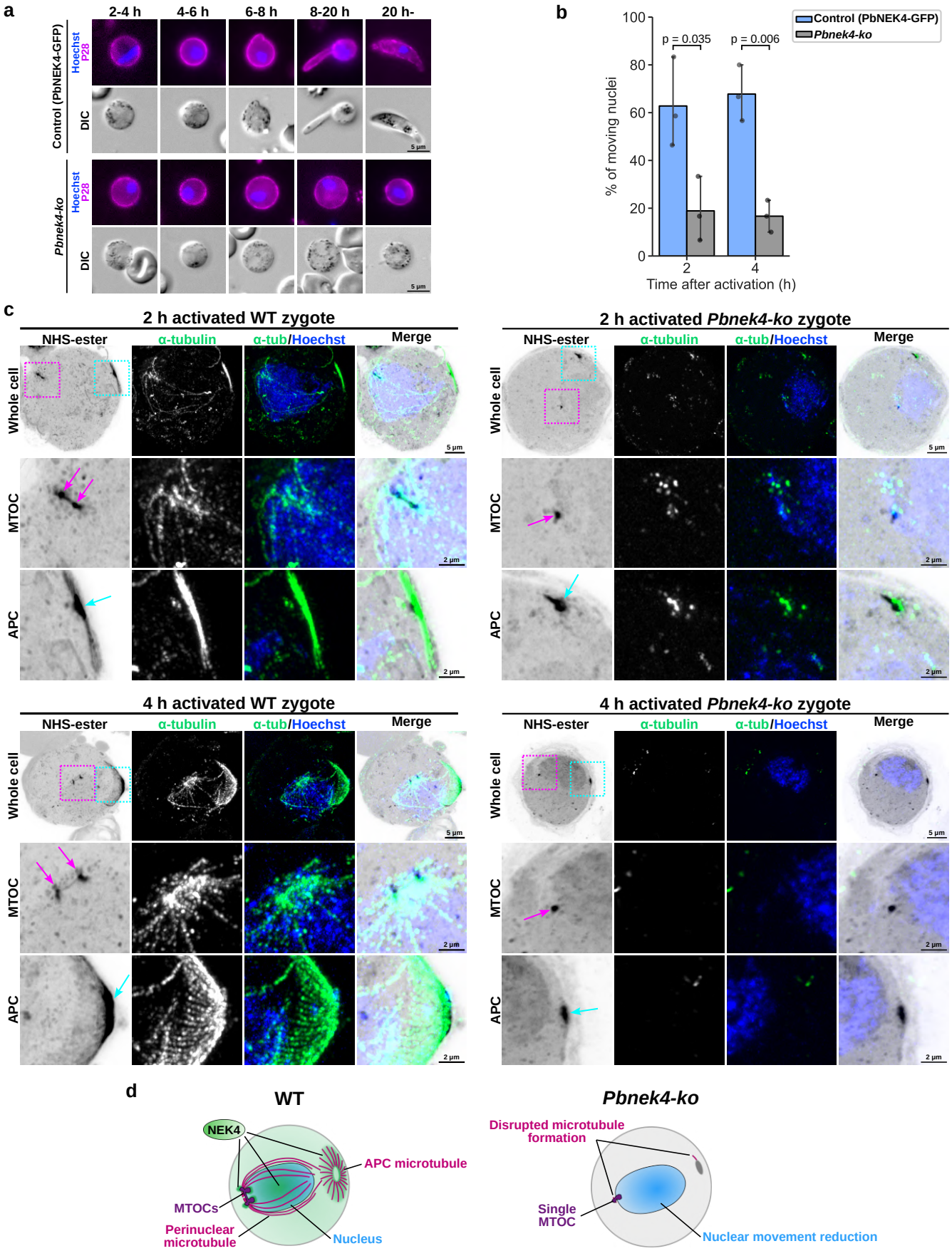
a
2-4 h
4-6 h
6-8 h
8-20 h
20 h-
Control (PbNEK4-GFP)
Hoechst P28
DIC
Pbnek4-ko
5 µm
b
Control (PbNEK4-GFP)
Pbnek4-ko
p = 0.035
p = 0.006
% of moving nuclei
Time after activation (h)
c
2 h activated WT zygote
2 h activated Pbnek4-ko zygote
4 h activated WT zygote
4 h activated Pbnek4-ko zygote
NHS-ester
α-tubulin
α-tub/Hoechst
Merge
Whole cell
MTOC
APC
2 µm
d
WT
Pbnek4-ko
NEK4
APC microtubule
MTOCs
Perinuclear microtubule
Nucleus
Disrupted microtubule formation
Single MTOC
Nuclear movement reduction

Figure 4

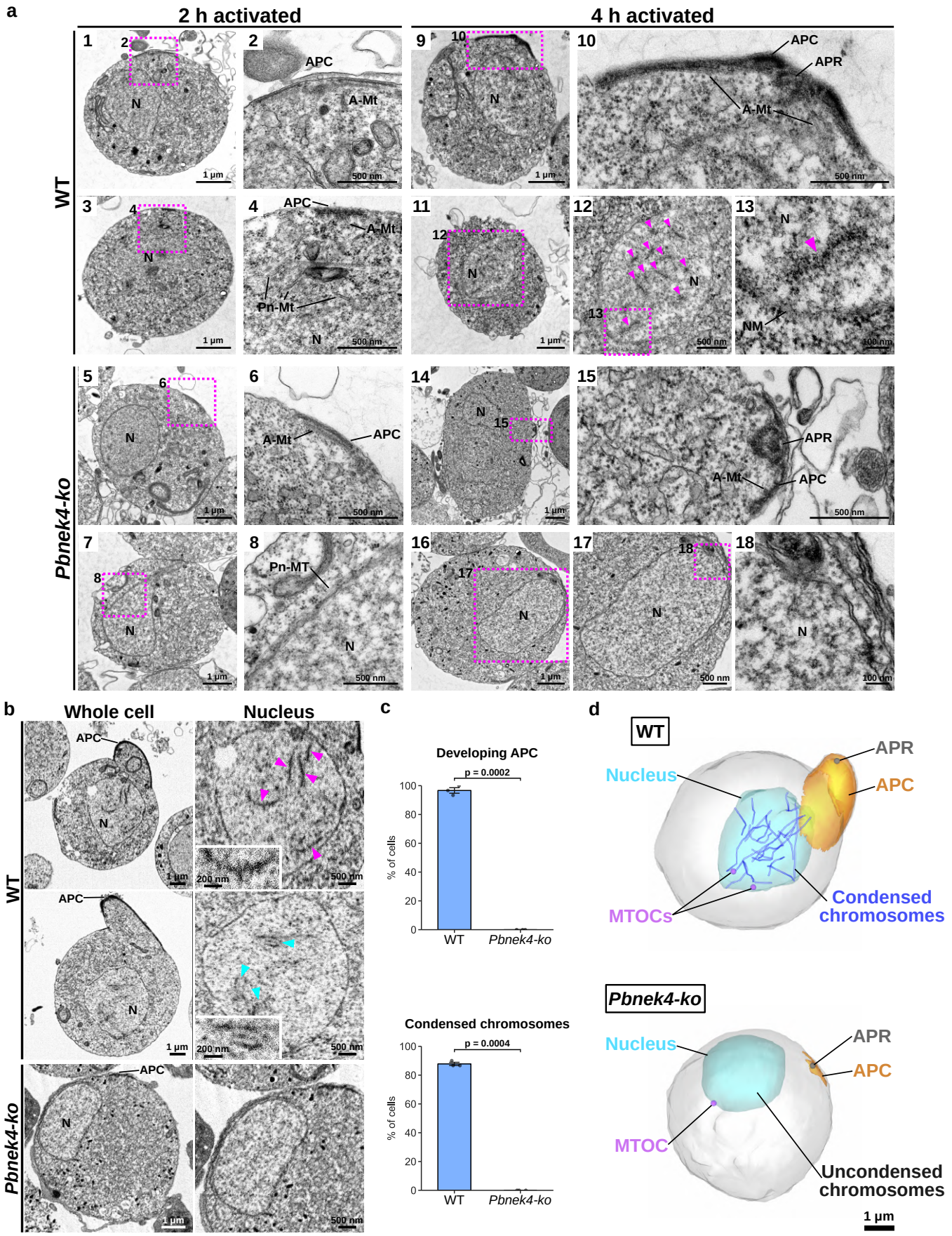
a
2 h activated
4 h activated
WT
Pbnek4-ko
N
APC
APR
A-Mt
Pn-Mt
NM
1 µm
500 nm
100 nm
b
Whole cell
Nucleus
200 nm
c
Developing APC
p = 0.0002
% of cells
WT
Pbnek4-ko
Condensed chromosomes
p = 0.0004
d
Nucleus
APR
APC
MTOCs
Condensed chromosomes
MTOC
Uncondensed chromosomes
1 µm

Figure 5

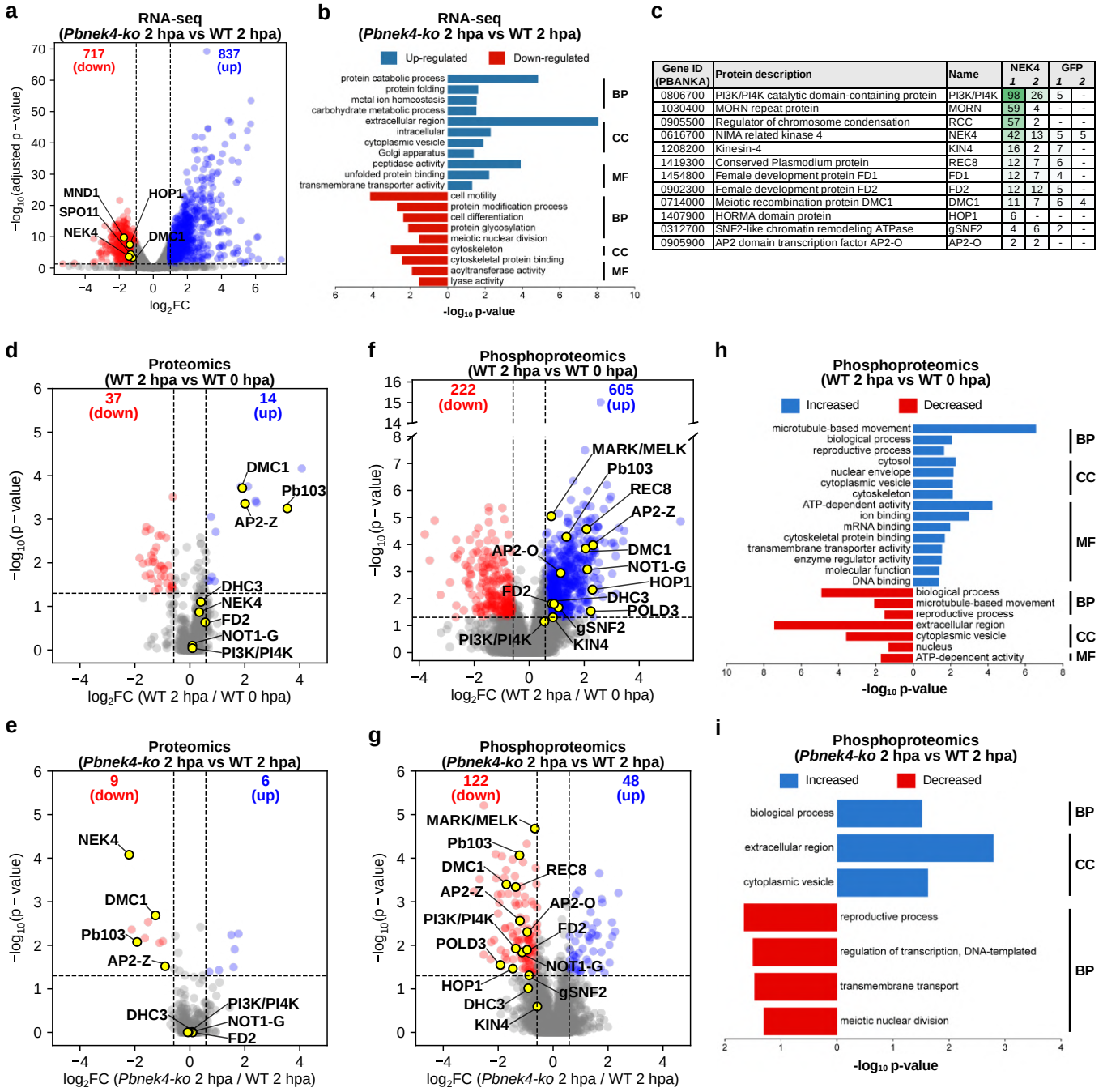

Gene ID (PBANKA)	Protein description	Name	NEK4 1	NEK4 2	GFP 1	GFP 2
0806700	PI3K/PI4K catalytic domain-containing protein	PI3K/PI4K	98	26	5	-
1030400	MORN repeat protein	MORN	59	4	-	-
0905500	Regulator of chromosome condensation	RCC	57	2	-	-
0616700	NIMA related kinase 4	NEK4	42	13	5	5
1208200	Kinesin-4	KIN4	16	2	7	-
1419300	Conserved Plasmodium protein	REC8	12	7	6	-
1454800	Female development protein FD1	FD1	12	7	4	-
0902300	Female development protein FD2	FD2	12	12	5	-
0714000	Meiotic recombination protein DMC1	DMC1	11	7	6	4
1407900	HORMA domain protein	HOP1	6	-	-	-
0312700	SNF2-like chromatin remodeling ATPase	gSNF2	4	6	2	-
0905900	AP2 domain transcription factor AP2-O	AP2-O	2	2	-	-

j

Function	Gene ID (PBANKA)	Protein description	Name	Phosphoproteomics (log_2FC) *Pbnek4-ko* 2 h vs WT 2 h	Phosphoproteomics (log_2FC) WT 2 h vs WT 0 h	Proteomics (log_2FC) *Pbnek4-ko* 2 h vs WT 2 h	Proteomics (log_2FC) WT 2 h vs WT 0 h	Phosphopeptide sequence
Meiosis	0714000	Meiotic recombination protein DMC1	DMC1	-1.70	2.05	-1.25	1.91	SASKVALTTNVEEITK
	1407900	HORMA domain protein	HOP1	-1.46	2.30	-	-	TNGYESEQSK
	1419300	Conserved Plasmodium protein	REC8	-1.36	2.08	-	-	ITHQNSLLQQIFTNSTFNDTSK
DNA replication	1242400	Conserved Plasmodium protein	POLD3	-1.92	2.24	-	-	DNNATPK
Sexual development	1134900	Zinc finger protein	Pb103	-1.22	1.35	-1.92	3.55	INEAYVSNNFEEVDINQYCEK
	0612400	AP2 domain transcription factor AP2-Z	AP2-Z	-1.21	2.32	-0.90	2.01	ISNIPSDYAEKEK
	0943100	CCR4-NOT transcription subunit NOT1-G	NOT1-G	-1.13	2.11	0.08	0.09	LYSSPKPLTLIYK
	0902300	Female development protein FD2	FD2	-0.95	0.83	0.10	0.56	NNSHDIR
	0905900	AP2 domain transcription factor AP2-O	AP2-O	-0.94	1.14	-	-	NYTPNFNLQK
	0312700	SNF2-like chromatin remodeling ATPase	gSNF2	-0.87	1.06	-	-	KYSEFSEPSNILSVSTK
MTOC/MTs	0806700	PI3K/PI4K catalytic domain-containing protein	PI3K/PI4K	-1.36	0.55	-0.05	0.09	KELNETLEIYR
	1305200	Serine/threonine protein kinase	MARK/MELK	-0.66	0.80	-	-	NNSNIEYFLK
	0214000	Dynein heavy chain	DHC3	-0.91	0.90	-0.08	0.40	SNSEKYGENNYPHGMR
	1208200	Kinesin-4	KIN4	-0.58	0.86	-	-	LYNLDSIKNSK
	0616700	NIMA related kinase 4	NEK4	-	-	-2.21	0.34	-

Figure 6

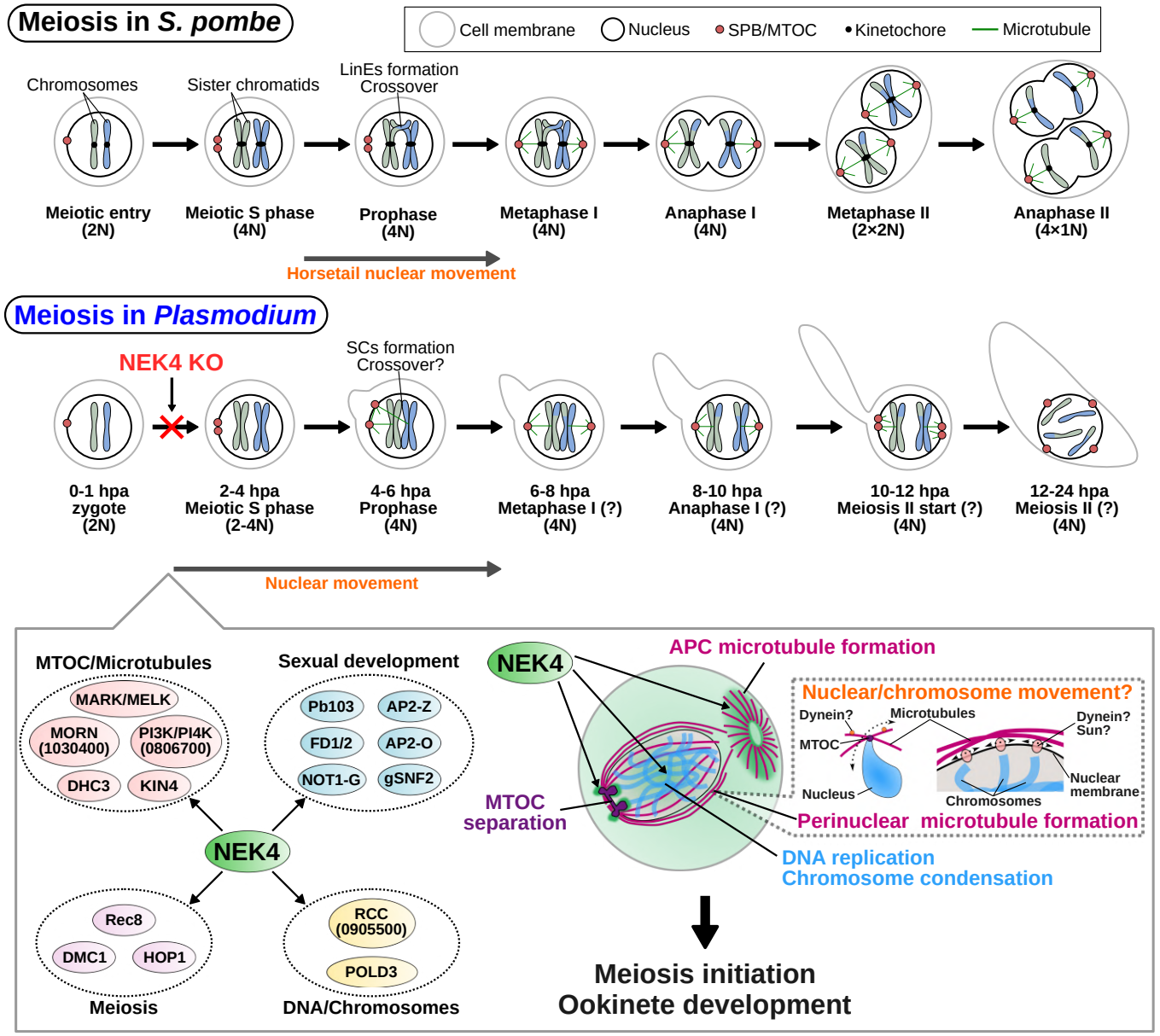
Meiosis in S. pombe
Cell membrane
Nucleus
SPB/MTOC
Kinetochore
Microtubule
Chromosomes
Sister chromatids
LinEs formation
Crossover
Meiotic entry (2N)
Meiotic S phase (4N)
Prophase (4N)
Metaphase I (4N)
Anaphase I (4N)
Metaphase II (2×2N)
Anaphase II (4×1N)
Horsetail nuclear movement
Meiosis in Plasmodium
NEK4 KO
SCs formation
Crossover?
0-1 hpa zygote (2N)
2-4 hpa Meiotic S phase (2-4N)
4-6 hpa Prophase (4N)
6-8 hpa Metaphase I (?) (4N)
8-10 hpa Anaphase I (?) (4N)
10-12 hpa Meiosis II start (?) (4N)
12-24 hpa Meiosis II (?) (4N)
Nuclear movement
MTOC/Microtubules
MARK/MELK
MORN (1030400)
PI3K/PI4K (0806700)
DHC3
KIN4
Sexual development
Pb103
AP2-Z
FD1/2
AP2-O
NOT1-G
gSNF2
NEK4
Rec8
DMC1
HOP1
Meiosis
RCC (0905500)
POLD3
DNA/Chromosomes
NEK4
APC microtubule formation
Nuclear/chromosome movement?
Dynein?
Microtubules
Dynein? Sun?
MTOC
Nucleus
Chromosomes
Nuclear membrane
MTOC separation
Perinuclear microtubule formation
DNA replication
Chromosome condensation
Meiosis initiation
Ookinete development